A Small Mobile Molten Salt Reactor (SM-MSR) For Underdeveloped Countries and Remote Locations

By:

William A Casino
Kirk Sorensen
Christopher A Whitener

Graduate Design Team Entry
American Nuclear Society
Student Design Competition

April 25, 2007

Faculty Advisor
Dr. M.L. Grossbeck

Nuclear Engineering Department
The University of Tennessee

Abstract

One of the objectives of the Global Nuclear Energy Partnership (GNEP) Initiative is to design, develop, and deploy small-scale reactors that are cost-effective, secure, and well-suited to conditions in developing nations. These reactors must strive to perform as well as possible in as many operational aspects as possible in order to accomplish favorable economic performance. They must allow a customer country to incrementally enter into the use of nuclear energy. They should be designed to serve small and weakly-linked power distribution grids. They should also be attractive for use in district heating and water-desalination projects. They must strive to maximize design aspects which correspond to safety and non-proliferation objectives as defined by the International Atomic Energy Agency and the US Nuclear Regulatory Commission. They should maximize fuel-cycle lifetimes in order to reduce refueling and maintenance operations as much as is practical. They should additionally exhibit robust performance as either a baseload or load-following plant, and they should be easy to operate and maintain.

The objective of this project is to design such a reactor that can be transported by truck to a remote location and operated for an extended period of time with minimal interactive support. The target steady state electric power production goal is 100 MW electric.

Table of Contents

List of Figures

List of Tables

List of Equations

1.0 Introduction

One of the objectives of the Global Nuclear Energy Partnership (GNEP) Initiative is to design, develop, and deploy small-scale reactors that are cost-effective, secure, and well-suited to conditions in developing nations. These reactors must strive to perform as well as possible in as many operational aspects as possible in order to accomplish favorable economic performance. They must allow a customer country to incrementally enter into the use of nuclear energy. They should be designed to serve small and weakly-linked power distribution grids. They should also be attractive for use in district heating and water-desalination projects. They must strive to maximize design aspects which correspond to safety and non-proliferation objectives as defined by the International Atomic Energy Agency and the US Nuclear Regulatory Commission. They should maximize fuel-cycle lifetimes in order to reduce refueling and maintenance operations as much as is practical. They should additionally exhibit robust performance as either a baseload or load-following plant, and they should be easy to operate and maintain.

Achieving these objectives with current nuclear technologies, as embodied by the pressurized-water reactor, would be extremely difficult. Today's nuclear technologies require a level of precision in control and training that would be difficult to expect in a small and possibly underdeveloped country. Therefore, it is unsurprising that we must look for solutions to the aggressive set of design requirements outside of the traditional bounds of mature nuclear technology.

Safety is a paramount concern in this reactor design. The first and most important safety feature of a reactor is its reactivity response. The reactor must possess a strongly negative temperature coefficient of reactivity, to protect the reactor against reactivity excursions and to provide responsiveness to the electrical load. This negative temperature coefficient must be innate to the design and impervious to external changes to the reactor, such as damage or sabotage. All such events must reduce the reactivity level of the reactor, not increase it.

The second most important safety feature is passive decay heat removal. In a solid-core reactor, the inability to remove decay heat can lead to fuel melting, coolant channel blockage, and vessel failure. Newer reactor designs attempt to improve the decay removal system by adding coolant systems that are passive in operation through a greater gravitational potential or a large thermal capacity. Like reactivity safety, damage or sabotage should not undermine the ability to passively remove decay heat in all circumstances.

Other safety features concern the chemical stability of fuel and coolants to potential external chemical reactions. A reactor that has reactivity and decay heat safety is of little value if the entire system could be destroyed through chemical reaction with commonly-occurring ambient materials like air and water. Again, one must consider both damage and sabotage in these considerations.

Safety is also related to reactor complexity. A reactor with a minimum of systems that can fail in the first place is preferable to a system full of components engineered and demonstrated to high reliability. Reductions in reactor complexity pay off across the board in the reactor design, leading to greater safety, simplified development, reduced cost, and easier operation and disposal.

Economy in operation is critical to a small reactor. Each unit mass of the reactor system must do a great deal if the reactor is to be portable and power-rich. Current reactors that rely on heavy pressure vessels, large containments, complex heat-removal systems, and technically-trained personnel will not be able to be exported economically to the developing world.

The reactor must be reliable. It must be able to not only follow the electrical load exerted by the grid but

must be able to shed its load quickly in the event of severe grid instability and then reassume the load in a brief period of time. Today's reactors struggle with restart after a scram because of the accumulation of xenon-135 in their core and the ensuing change in reactivity. A reactor that can achieve the ambitious goals of the GNEP program cannot be hobbled by xenon transients during shutdown and must be able to handle load-shedding without a scram.

Finally, the reactor must be inexpensive to develop. New fuel forms must be able to be qualified quickly and inexpensively, ideally in existing test facilities. Power conversion systems should be able to be developed in parallel to the reactor using non-nuclear heating. Reactor components should be rugged and lightweight, which will only be possible if the reactor operates at lower pressures than current pressurized-water reactor technology. Safety procedures should be straightforward and easy to develop because the vast majority of failure scenarios should be designed out of the reactor from the outset. External reactions between reactor components, fuels, and coolants should be minimized or eliminated. The reactor must be simple.

The objective of this project is to design a reactor that meets these goals and can be transported by truck to a remote location and operated for an extended period of time with minimal interactive support. The target steady state electric power production goal is 100 MW electric. The reactor technology chosen to accomplish these goals utilizes a liquid-fluoride salt as the primary core fluid, with another fluoride salt as the core coolant and a closed-cycle helium gas-turbine as the power conversion system. These technologies can achieve the goals that have been laid out for this project and deliver a reactor of superior safety, performance, flexibility and portability that can be developed in a shortened period of time. The design is named the ***S***mall ***M***obile ***M***olten ***S***alt ***R***eactor (SMMSR)

2.0 Overview of the SMMSR Design

The overall layout of the SMMSR system is shown in **Figure 1**. The primary containment module is placed below grade in order to take advantage of earth for shielding and intruder prevention. It contains the criticality chamber which, since the SMMSR is an epithermal system, is a right circular cylinder graphite pile. The primary containment module also contains the vertical lengths of the hot and cold leg piping which is connected to the primary to intermediate loop heat exchanger. The primary containment module is 25 meters tall in order to allow sufficient height to support natural circulation of the primary coolant. By not using a primary circulating pump, the probability of mechanical or electrical failures is reduced which supports an extended operating life cycle. The primary to intermediate heat exchanger is at the top of the primary containment module and allows for salt addition, fission product gas removal, thermal expansion of the primary fluid, and addition of fuel to the liquid fuel salt, as well as heat transfer to the intermediate loop system. The primary containment module is capped off with a large biological shield which allows the region of space immediately above it to be a 40 hour per week occupancy zone, as well as providing an impenetrable cap atop the module to mitigate human intrusion into the system. The primary to intermediate heat exchanger has hot and cold leg piping which bypasses the biological shield and connects to the secondary loop module which is placed at grade level. The secondary loop exists in order to isolate the environment and the power cycle from the radioactive primary fuel salt in the unlikely event of a primary to secondary leak. The secondary loop uses a circulating pump and a secondary to helium heat exchanger to transfer thermal energy from the primary system to the power cycle. The heat exchanger is divided up into three approximately equal sized sections to extract heat from the secondary salt and transfer it to the helium working fluid of the power conversion system. The three heat exchangers are collocated within the secondary module. The power conversion system is a helium Brayton system which uses a double re-heat process in order to maximize efficiency. The power cycle is connected to a heat sink mechanism which will be site specific. It is anticipated that the SMMSR will be called upon to support district heating and water desalinization as a part f the GNEP mission under which it will be deployed; therefore the heat sink system will incorporate these features as needed. The intermediate loop

module and power conversion cycle components need not be located on top of the biological shield, but close proximity location of connected systems will minimize environmental heat losses and promote resource efficiency.

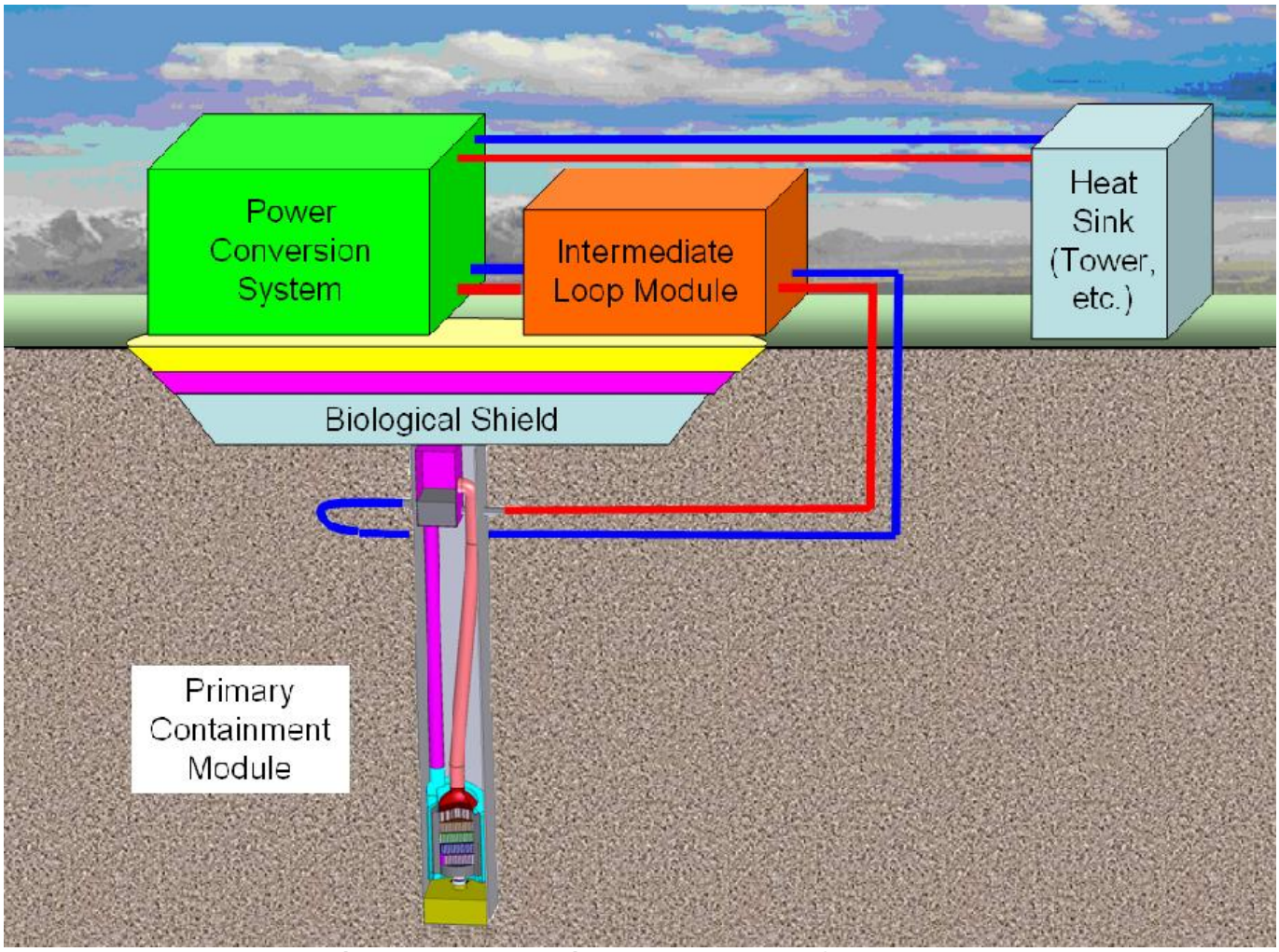

Figure 1: System and Component Layout for SMMSR

3.0 Primary System

3.1 System Overview

The primary system consists of the primary containment structure, the moderator chamber, the primary loop piping and components, the primary-to-secondary heat exchanger, the core safety dump tanks and associated components, the upper biological shield assembly, the fission-product gas collection system, and supporting piping and valves for fuel salt addition and removal. It also contains detection system components for power monitoring instrumentation as well as many other auxiliary systems and components necessary to support the operations of the SMMSR.

The primary system is designed to operate in a semi-autonomous manner in that no operator action is needed during normal steady state and transient operations. The system requires active monitoring, and regular fuel addition as a part of the normal scope of operations, but the core and fuel salt system require no control actions. The system has no primary coolant pumps. Natural circulation was adopted in order to simplify operations, enhance long-term operational stability, and ensure high availability. No control devices such as rods, soluble poisons, or moveable reflectors are needed. The reactor system regulates

power and temperature autonomously by taking full advantage of the unique properties of liquid fuels. The system contains no pressurization mechanism, as the fuel salt is capable of remaining in a liquid state at temperatures up to 1700K and atmospheric pressure. The primary coolant system is somewhat self-cleaning in that many features have been incorporated into the design layout of the system in order to optimize solid and gaseous byproduct removal. The overall temperature safety system uses a passive freeze valve design to place the system into a fail-safe state upon initiation of an excessive over-power or over-temperature accident. Detailed descriptions of each SMMSR operating feature are discussed in the related component discussions to follow. It is anticipated that the primary system will be permanently sealed in the primary containment structure. No human intrusion will be necessary or possible for the anticipated 30-year lifespan of the system. The primary system and components are illustrated in **Figure 2**.

The size of the system is limited by that which can be transported over land using a heavy transporter. The special permit parameters were chosen as an upper limit for the primary containment structure outer dimensions, and after the design was completed, a total mass and size calculation was performed to check for compliance with **Table 1** limitations. The primary system module is illustrated in **Figure 3** positioned horizontally for overland transport.

Table 1: Transportation Limitations for Overland Transport of Large Payloads

Parameter	Units	Standard Tractor Trailer	Special Permit Tractor Trailer	Heavy Haul Transport
Length	feet / meters	53 / 16.15	125 / 38.1	-
Width	feet / meters	8.5 / 2.59	16 / 4.88	-
Height	feet / meters	13.5 / 4.11	15.5 / 4.72	-
Weight	pounds / metric tons	80,000 / 36.29	180,000 / 81.65	1,000,000 / 453.6

The mass of the structure is 410 metric tons. The derivation of the primary system mass and volume is detailed in **Section 6.1.2**, and summary results are shown in **Table 2**. The determination of these calculated values is discussed in each components discussion section. The system is to be transported to the site with no fuel salt in it and no biological shield installed. The system will be filled and tested after being positioned within its operating silo below grade. Further details about the transport, assembly set up, testing, disassembly, and decommissioning are discussed in section **6.0**.

Table 2: Mass and Volume of Components within the Primary Containment Module

	Mass			Volume
Component	**Kilograms**	**Metric Tons**	**US Tons**	**m^3**
Moderator Chamber	195816	196.0	216.0	-
Primary Piping	6914	6.9	7.6	0.78
Primary to Secondary Heat Exchanger	157116	15.7	17.3	-
Core Dump Tank	23047	23.0	25.0	2.6
Primary Containment Structure	168401	168.4	186.0	21.4
Shipping Total	409899	410	454.0	-

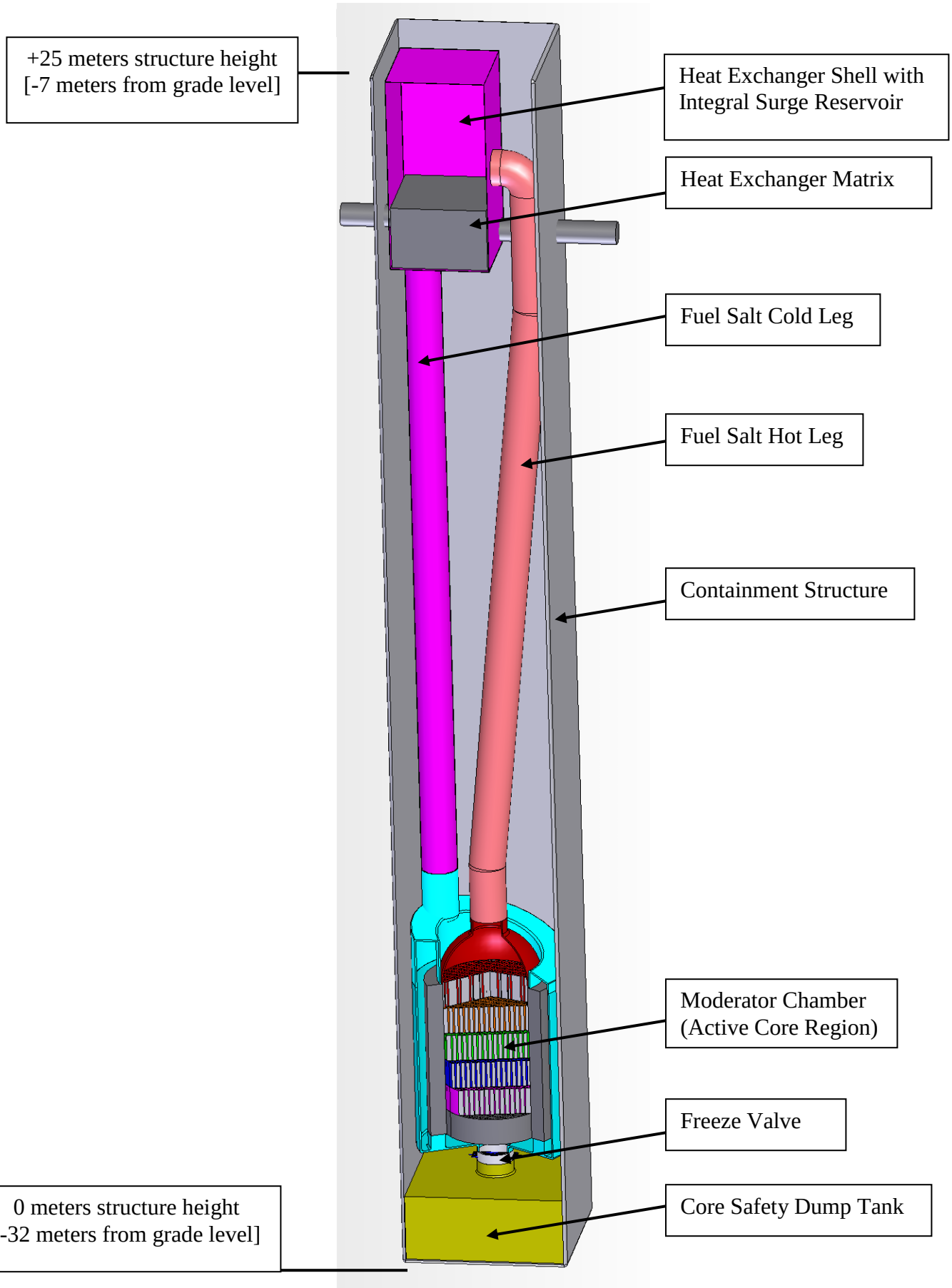

Figure 2: SMMSR Primary System and Components

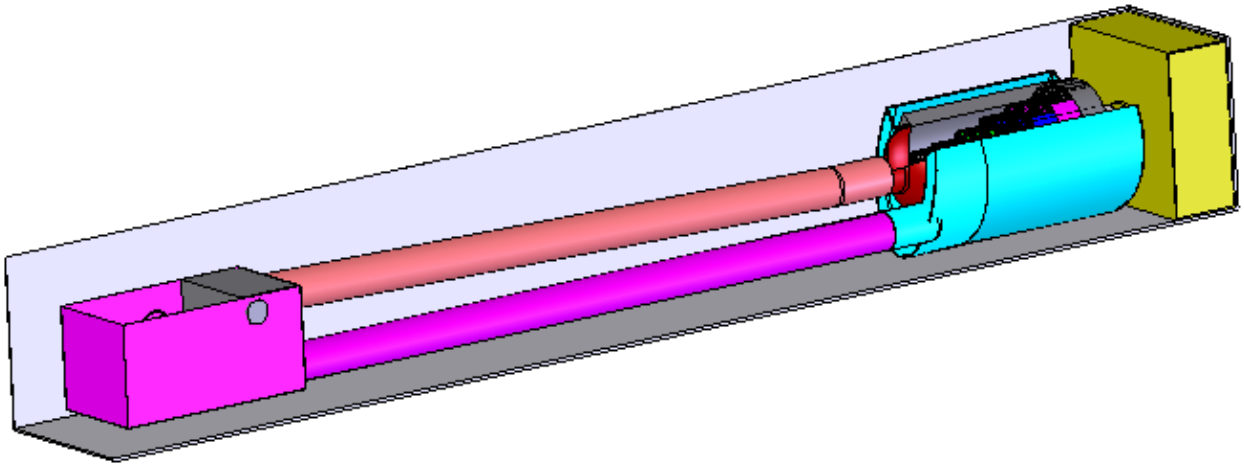

Figure 3: Primary System Module Positioned Horizontally for Transport

3.2 Components

3.2.1 Primary Containment Structure

As was mentioned in Section 3.1, the primary containment structure is sized so as to be transportable over land by heavy transport. The primary containment structure is a right parallelepiped with a base dimension of 4.88 square meters by 25 meters in height. The structure is made of a carbon-steel alloy with a Hastelloy-N plated interior surface. Hastelloy-N alloy is a nickel-base alloy that was invented at Oak Ridge National Laboratories as a container material specifically for molten fluoride salts. It is oxidation resistant to hot fluoride salts up to a temperature of 1150K (**Reference 12**) and also exhibits good oxidation resistance in air. Hastelloy-N can be welded and forged. As an alloy, Hastelloy-N can be supplied, to order, from commercial manufacturers in the forms of sheet, plate, bar rod along with welded and seamless pipe and tubing. The use of this plating ensures corrosion resistance in case of fuel or secondary salt leakage onto the interior surface. The alloy and plating of all sides of the structure are 1 centimeter thick and structural rigidity is accomplished by use of a skeleton of beams and supports. The lower surface and the lower portion of the side surfaces are provisioned with an emergency decay heat removal system for when the emergency core dump tank is used. Further discussion of this heat removal system is located in Section **3.2.5**. The structure has a removable upper shadow biological shield which fits over the upper lid. The shadow shield is detailed in **Section 3.2.6**. The upper lid is the only provided human ingress/egress point, and when the biological shield is in place, the primary containment structure cannot be accessed with out the use of heavy lifting equipment or cutting through one of the unshielded side bulkheads. Once the system has been operated at full power for a short period of time, the fuel salt becomes highly activated which inhibits direct human contact. This design feature supports the GNEP objective of enhancing proliferation resistance and site security through passive means. In order for this approach to be practical, the primary system must be designed in such a way that normal and emergency operations can be performed without ever needing direct access to the primary components. The SMMSR is designed to achieve that goal.

3.2.2 Primary Coolant Loop

3.2.2.1 Fuel Salt

The fuel salt used in the SMMSR is consists of uranium tetrafluoride dissolved in a solution of lithium and beryllium fluorides, as is shown in **Figure 4**.

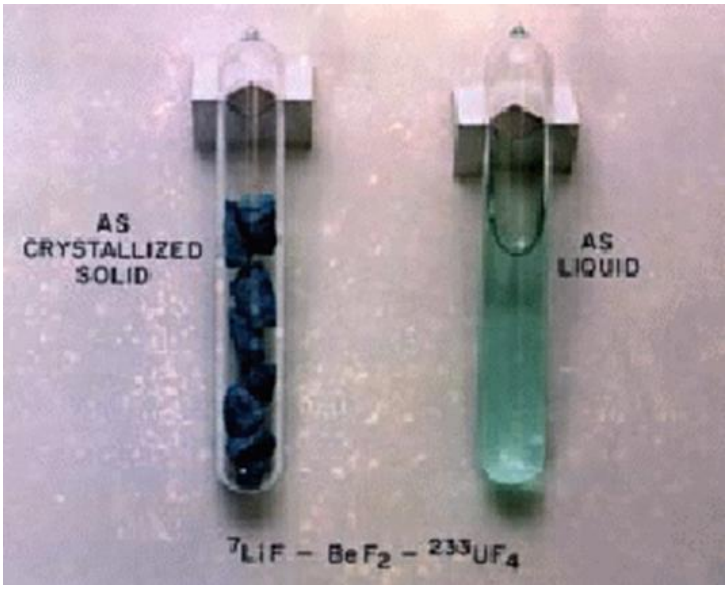

Figure 4: Frozen and Liquid Fluoride Salts of Lithium, Beryllium, and Uranium

The lithium fluoride is highly-enriched in the lithium-7 isotope, which is very important to reduce parasitic neutron capture in lithium-6. The composition of the fuel salt, in terms of mole percentages, is 67% lithium fluoride, 30.5% beryllium fluoride, and 2.5% uranium tetrafluoride. (LiF [67]-BeF_2 [30.5]-UF_4 [2.5]). This base solvent is commonly called "FLiBe". The initial charge of UF_4 is enriched to 5 w/o U235 and is maintained at 2.5 mole fraction throughout the life of the system via continuous UF_4 addition which is discussed in detail in section **6.2.2**. Key thermo-physical properties of the fuel salt LiF [67]-BeF_2 [30.5]-UF_4 [2.5] and the base solvent LiF [66]-BeF_2 [34] are listed in **Table 3**.

Table 3: Key Thermo-Physical Properties of FLIBE-UF_4 and FLIBE [1 and 2]

Property	**LiF[67]-BeF2[30.5]-UF4[2.5]**	**LiF[66]-BeF2[34]**
Melting Point (K / C)	737 / 463	733 / 459
Boiling Point (K / C)	1673 / 1400	1703 / 1430
Density (kg/m^3) @ 973 K	2100	1940
Thermal Expansion (per K)	1.90E-4	4.88E-4
Density Function (input temp in K)	$\rho(T)=2.1 - 1.9E\text{-}4*(T - 973)$	$\rho(T)=2.28 - 4.88\text{-}4*(T - 973)$
Viscosity (kg / m-sec)@973 K	0.0055	.0052
Thermal Conductivity (Watt / m-K)	1.0	1.0
Specific Heat (kjoule / kg-K)	2.4	2.34
Prandtl Number (unit less)	7	13.525

Determination of Total Fuel Salt Volume and Mass

The three main components of the primary system considered in fuel salt volume are the vessel, the primary heat exchanger and the primary piping. The primary heat exchanger is a compact design and requires a low inventory of fuel salt for heat transfer. The total volume of the heat exchanger is 10 m^3 and contains 3.34 m^3 of fuel salt. The active region of the core is 3 meters in diameter and 6 meters in height. A 7 meter height and a 4 meter diameter are assumed to allow for plenums, distribution headers and a salt blanket in the downcomer region of the core. This results in 88 m^3 of core volume. In the core region, the ratio of graphite to salt is 90% graphite to 10% salt by volume, so there is ~ 9 m^3 of fuel salt in the core. The primary piping has an inside diameter of 0.5 meter and a total length of 23 meters. This gives a volume of 4.5 m^3 in the primary piping. The total inventory of primary fuel salt is 16.8 m^3. Using the density of 2100 kg/m^3 gives a total mass of ~35,300 kg of fuel salt (~40 US tons).

3.2.2.2 Piping System

The primary system piping is constructed of Hastelloy-N alloy to ensure chemical compatibility with the liquid fluoride fuel salt. The system has sacrificial metal anodes located throughout to allow plate out of fission product noble metals. The piping is structured so as to have smooth radius bends and minimal frictional losses to optimize the efficiency of the natural circulation of the primary (see **Figure 2**). Natural circulation is discussed in detail in **Section 3.2.2.3**.

Piping Wall Thickness

The primary loop in this nuclear system design is not pressurized but is intended to operate at near atmospheric pressure or 0.1 MPa. Since natural circulation is used for movement of the primary fuel salt without the added pressure of a mechanical pump, the forces acting on the interior surfaces of the vessel are only those due to hoop stress and longitudinal stress from in the piping, and only that induced by the hydrostatic force of the molten salt as a function of height and density. The wall thickness calculation is based on the more conservative of the hoop stress or the longitudinal stress calculations to follow.

Hoop Stress Determination

The system minimum height from the center of the core to the center of the heat exchanger determined for natural circulation is 14 meters giving a total piping length equivalent from the bottom of the vessel to the top of the heat exchanger of 18.5 meters. The cold leg density of 2023 kg/m^3 is also used. The most conservative design limit for Hastelloy-N at high temperatures to 1000K from Boiler Code Design Data in **Reference 12** is 11 MPa (1600 psi). The vessel thickness required from hoop stress is given by **Equation 1**:

Equation 1: Hoop Stress

$$\sigma_h = (p \cdot r)/t$$

where

σ_h = hoop stress, p = pressure in pipe, r = radius of vessel, t = thickness of pipe

$p = \rho_c \, g \, H = 2023 \text{ kg/m}^3 \cdot 9.8 \text{ m/s}^2 \cdot 18.5 \text{ m} = 366770 \text{ Pa} = 0.37 \text{ MPa}$
where

p = hydrostatic pressure, ρ_c = density of fuel salt in cold leg, g = gravitational acceleration and H=height

σ_h = 11 MPa conservative design limit of Hastelloy-N

which gives

11 MPa = (0.37 MPa · 0.25)/t and t= approximately 1.0 centimeter thick.

This is conservative in that it assumes the entire distance from the top of the heat exchanger to the bottom of the vessel is a single pipe with diameter of 0.5 meters.

Longitudinal Stress Determination

The longitudinal stress is half of the hoop stress using the same dimensions. **Equation 2** below also results in half of the thickness (~0.5cm). To provide a safety factor of two, the thickness of 2 cm is used for the primary piping hot and cold legs and the primary heat exchanger shell.

Equation 2: Longitudinal Stress

$$\sigma_l = (p \cdot r)/2t$$

A similar approach is used for the vessel thickness determination. The thickness from hoop stress for the vessel is

$$p = \rho c\, g\, H = 2023\ kg/m^3 \cdot 9.8\ m/s^2 \cdot 7\ m = 138778\ Pa = 0.14\ MPa$$

11 MPa = (0.14 MPa · 1.5)/t and t= approximately 2.0 centimeter thick.

Again, longitudinal stress would be half of the hoop stress and result in a thickness of ~1.0 cm. To provide further safety for containment of the primary fuel system which is the initial barrier to release of fission products, and for structural support of the vessel internals, an additional 1.2 cm is added, to give a total of 3.2 cm (1.25 inches) thickness for the vessel walls based on the hoop stress calculation. As a result, the primary piping thickness is conservatively determined to be 2.0 cm thick and the vessel is 3.2 cm thick (1.25 inches).

3.2.2.3 Natural Circulation

Natural circulation is a desired criterion in the primary coolant loop design of this project. With natural circulation, heat transfer from the source to the sink can be accomplished without the addition of a mechanical pump. The necessity of a mechanical pump would require a penetration into the primary system which increases the probability of system leakage through the system to pump interface seal. It also introduces an increase in the probability of needing to perform onsite maintenance. The maintenance of the pump, either routine or as on-demand repair could also require entry into the containment structure of the primary system. At least two of the important design criteria for this project were: (1) minimal onsite maintenance resulting in an essentially autonomous reactor since there is no trained workforce for complicated system maintenance, (2) a proliferation resistant design which could be translated into a requirement for a sealed encapsulated primary system without a requirement for entry. Natural circulation in the primary system would support both of these design goals. The schematic of natural circulation is demonstrated in **Figure 5** using a uniform diameter rectangular loop with adiabatic pipes.

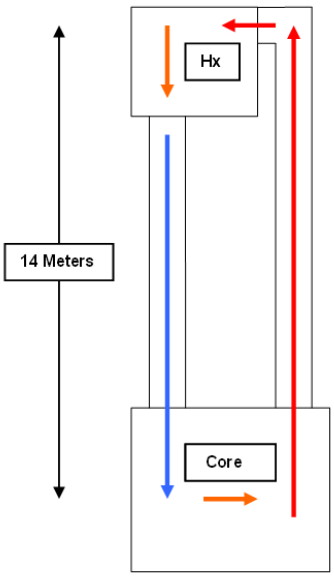

Figure 5: SMMSR Natural Circulation

At the core (heat source), the fuel salt absorbs heat which reduces the salt density. It becomes lighter than the salt in the cold leg piping and rises. At the primary heat exchanger (heat sink), the fuel salt rejects heat becomes heavier and sinks, making possible natural circulation. The design inlet temperature of the core is 800K and the outlet design temperature is 1000K resulting in a ΔT of 200K. The heat exchanger design inlet temperature is 1000K and the outlet design temperature is 800K also resulting in a ΔT of 200K. The source and sink conditions are maintained constant achieving a steady state condition where the heat absorbed at the source is equal to the heat rejected at the sink (ΔT=200K at both core and primary heat exchanger). Under steady conditions a density of ρ_h (hot) is assigned to the vertical leg with upward flow and ρ_c (cold) to the other vertical leg with downward flow. The hydrostatic pressure, P_c and P_h located at the bottom of each flow path are calculated with **Equation 3** and **Equation 4** below:

Equation 3: Hydrostatic Pressure, P_c

$$P_c = \rho_c \cdot g \cdot H$$

Equation 4: Hydrostatic Pressure, P_h

$$P_h = \rho_h \cdot g \cdot H$$

Where H is the height and g is the acceleration due to gravity. Since the cold leg salt density is greater than the hot leg salt density, the corresponding cold leg pressure head is greater than the hot leg pressure head. This pressure difference between the points provides the motive force for the flow. This induces natural convection heat transfer to reject heat from the salt as it flows through the heat exchanger. After multiple iterations of pipe diameter and height, heat exchanger size and Reynolds numbers, the height of 14 meters from the center of the core to the center of the heat exchanger is used for achievement of natural circulation. This assumes the vessel is 7 meters in height and the piping between the core and primary heat exchanger add an additional 11.5 meters giving a total column of 14 meters to the center of the heat exchanger. This results in enough driving force to overcome the calculated pressure losses in the main primary components. Environmental losses are considered minimal at full power operations and are ignored in the calculations. **Equation 5** was used with data from

Table 4 **4** to perform these calculations.

Equation 5: FLIBE+UF4 Density as a Function of Temperature (Reference 13)

$$\rho = 2413 - 0.488(T \text{ in } K)$$

$\rho_c = 2413 - 0.488\ (800) = 2023\ kg/m^3$

$\rho_h = 2413 - 0.488\ (1000) = 1925\ kg/m^3$

$P_c = \rho_c\, g\, H = 2023\ kg/m^3 \cdot 9.8\ m/s^2 * 14\ m = 277556\ Pa$

$P_h = \rho_h\, g\, H = 1925\ kg/m^3 \cdot 9.8\ m/s^2 * 14\ m = 264110\ Pa$

$P_a - P_b = \Delta P = 13446\ Pa$

A mass flow rate of 500 kg/s was the basis for the calculations in Table 4. The additional driving force after subtracting pressure losses is 3425 Pa (13446-10021) which is approximately 30% greater than equilibrium pressure and provides a safety margin in the natural circulation calculations.

Table 4: Pressure Loss for Primary Components

Component	Pressure Loss Type	Reynolds Number	Pressure Loss (Pa)
Primary Heat Exchanger Channels	Friction	309	6956
Primary Pipe to Heat Exchanger	Sudden Restriction	N/A	204
Heat Exchanger to Primary Pipe	Sudden Expansion	N/A	408
Primary Piping	Friction	231498	93
Core Channel	Friction	5642	24
Primary Pipe to Core	Sudden Restriction	N/A	755
Core to Primary Pipe	Sudden Expansion	N/A	1510
90° elbows (16 m equivalent pipe)	Friction	231498	71
TOTAL PRESSURE LOSS			10021

3.2.3 Moderator Chamber

3.2.3.1 Introduction

The SMMSR is an epithermal-spectrum fluoride-salt-fueled system moderated by a matrix of solid graphite blocks. The blocks have a triangular pitch array of coolant/fuel salt channels which are configured vertically throughout the blocks. The blocks are arranged so as to form a right circular cylinder which is enclosed within an outer annulus of reflector graphite. The core blocks and outer reflector are surrounded by the fuel salt downcomer region. The inner structural components of the core are supported and contained by the outer vessel. The outer vessel also contains the upper inlet manifold, the lower inlet plenum on the lower extension below the active core region, and the upper outlet plenum on the upper extension above the active core region. The core diameter to the outer reflector region is 3 meters and the effective core height from the bottom to the top of the moderator block pile is 4.8 meters, creating an active core volume of ~34 cubic meters. At the rated full power of 240 MWt, the core power density is ~7 watts per cubic centimeter. The moderator to fissile ratio is set to an average 89.3% graphite to 10.7% fuel salt by volume, which makes the fuel region specific power density ~66 watts per cubic centimeter. This value is about 30% of a typical commercial GEN III PWR plant and affords the SMMSR the ability to reach the GNEP goal of 100 MWe for an operational period of 30 full power years while remaining within the given transportation based size and weight constraints. The reflector material is directly outside of the moderator block region and is a right circular cylindrical of graphite 0.75 meters thick. The reflector cylinder divides the upward flow of the core from the downward flow of the downcomer region. The down comer region is 5 cm wide and is bounded by the outer vessel, which is made of Hastelloy N and is 3.2 centimeters thick. There is a transition plenum at the bottom of the vessel which allows the incoming cold leg fuel salt to redirect upward into the active core region. The bottom of the vessel is equipped with a 1 meter diameter outlet flange projecting downward from the vessel low point which leads to the emergency core dump tank and freeze valve assembly. The moderator chamber assembly lay out is illustrated in **Figure 6**.

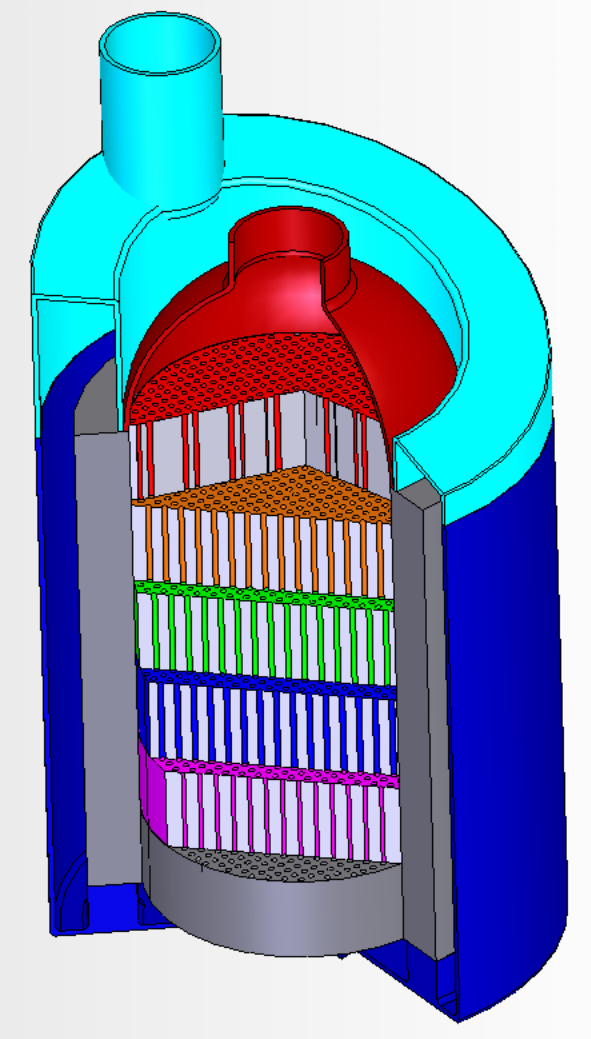

Figure 6: SMMSR Moderator Chamber and Plenums

The triangular pitch of the coolant/fuel salt channels is set at a constant 15.2 centimeters, which results in 390 fuel salt channels. The diameter of the fuel salt channel is not held axially constant. The radii of the fuel salt channels are set to 2.7 cm at the inlet of the lower core region and are gradually decreased to 2.6 cm at the outlet of the core. This variation, in combination with the steadily decreasing fuel salt density, effectively increases the moderator to fissile ratio as a function of axial position. The channels are shaped as right circular cones so as to minimize pressure drops and stepped changes in reactivity as the fuel salt flows upward through the core. This variation in moderator to fissile ratio acts in a similar manner as enrichment zoning, lumped burnable poison placement, and other strategic methods employed in solid fuelled cores in order to flatten radial and axial power distribution throughout the core.

3.2.3.2 Concept of Operation

The power generated by the fuel salt is controlled by three parameters; enrichment, density (which is a linear function of temperature), and moderator to fissile ratio. The enrichment is maintained constant via continuous or frequent batch addition, and the moderator to fissile ratio is fixed in each axial region of the core as a structural dimension of the coolant channels. The one variable parameter is the fuel salt density, which is a linear function of temperature. The density function for FLIBE+UF4 is shown in **Table 3**. In order to optimize the axial and radial power profile of the SMMSR, a series of KENO VI calculations were performed. In each calculation, an axial segment of the core was modeled with reflective upper and lower boundary conditions in which the coolant density, temperature, and moderator to fissile ratio were varied. The results of these calculations are shown in **Table 5**.

Table 5: KENO VI Analysis: Point Wise infinite Eigenvalue Values for Core Axial Zones

Temperature	K	783	823	863	903	943	983	1023
	C	510	550	590	630	670	710	750
Axial Location (meters)		0	0.8	1.6	2.4	3.2	4.0	4.8
Moderator Fraction	Salt Fraction							
90.2%	9.8%	-	-	-	1.0156	1.0124	1.0111	1.0079
90.0%	10.0%	1.0246	1.0200	1.0147	1.0126	1.0112	1.0078	1.0048
89.8%	10.2%	1.0194	1.0161	1.0118	1.0104	1.0081	1.0054	1.0011
89.6%	10.4%	1.0164	1.0147	1.0102	1.0075	1.0044	1.0016	0.9998
89.4%	10.6%	1.0149	1.0103	1.0066	1.0043	1.0017	0.9999	0.9970
89.2%	10.8%	1.0087	1.0080	1.0059	1.0007	0.9986	0.9960	0.9929
89.0%	11.0%	1.0069	1.0053	1.0006	0.9991	0.9962	0.9932	0.9910
88.8%	11.2%	1.0056	1.0027	0.9989	0.9971	0.9931	0.9909	0.9886
88.6%	11.4%	1.0036	0.9988	0.9962	0.9936	0.9904	0.9888	0.9812
88.4%	11.6%	1.0000	0.9950	0.9928	0.9901	0.9891	0.9799	-
88.2%	11.8%	0.9967	0.9933	0.9902	0.9878	0.9801	-	-

What can be observed from these results is that for a given fixed moderator to fissile ratio, the fuel salt temperature (density) is the driver of the reactivity balance for each axial region. For example, in the moderator to fissile ratio region of 88.8% to 11.2%, when the fuel salt is at 783K, the eigenvalue is 1.0056, which indicates a slight positive reactivity balance. The net positive reactivity in this axial region will result in power production and heat deposition into the fuel salt. As this happens, the fuel salt density will decrease as the fluid expands with temperature. By the time the fuel salt has reached a temperature of 863K, the thermal expansion of the fuel salt will have reduced the moderator to fissile ratio such that the axial region will now have a net negative reactivity balance. Now as the same fixed volume of fuel salt (at 863K) moves into the 89.2% to 10.8% axial region, the moderator to fissile ratio will increase sufficiently to yield a net positive reactivity balance. The energy generation rate in this region increases as before. This cycle will continue until the top axial region is reached in which the final core outlet temperature of 1023K is achieved. The proposed operating parameters for the 6 axial regions of the core are highlighted in **Table 5** as a function of moderator to fissile ratio. The color coded eigenvalues illustrate the region reactivity balance as a function of fuel salt temperature (density) in each region. The cooler, and hence denser, the fuel salt is as it enters the active core region, the more positive the reactivity balance will be and the higher the power production.

3.2.3.3 Temperature Coefficient

The system temperature (or power) coefficient is the key control parameter for the SMMSR operating concept. A KENO VI quarter core model was constructed for performing various core physics investigations for the SMMSR (see **Figure 7**). The calculation was set up at normal operating conditions and an effective eigenvalue calculation was performed. Then the system parameters were adjusted so as to reflect a plus 600K increase in the system temperature and associated densities. A second effective eigenvalue calculation was then performed, and the results were used in **Equation 6** to compute the system temperature coefficient.

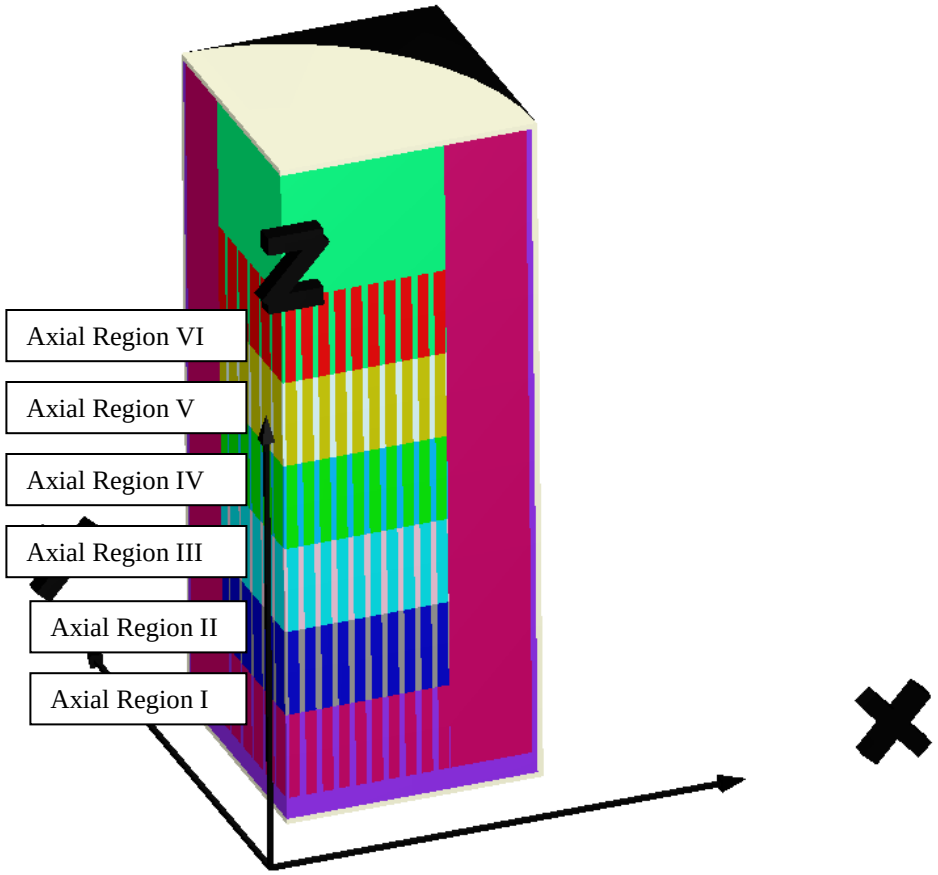

Figure 7: Keno VI ¼ Core Model of SMMSR

Equation 6: System Temperature Coefficient Relationship

$$\alpha_{STCR} = \frac{\left\{\frac{(k_{final} - k_{initial})}{(k_{final} * k_{initial})}\right\}}{\Delta Temperature}$$

The beginning of cycle normal operating condition system effective eigenvalue was calculated to be 1.09374 with a standard deviation of + or – 0.00093. The elevated condition eigenvalue was calculated to be 1.06954 with a standard deviation of + or – 0.00095. With a temperature perturbation of 600K, the system temperature coefficient was found to be -0.000034 delta-k/K or -3.4 PCM/K (percent milli-rho per K). By comparison, a typical PWR moderator temperature coefficient is on the order of -6 PCM/K.

3.2.3.4 Operating Life

Since continuous online fuel addition is possible with the SMMSR and the fuel salt is very robust, the operating lifetime of the system is limited only by restrictions on the maximum tolerable fluence that the moderator graphite can accumulate. **Reference 2** contains a relationship for estimating graphite fluence with local power density. The core power density is optimized by using the variable moderator to fissile ratio so as to reduce power peaking axially and radially. The net result is to spread the fluence impact of power operations more evenly throughout the entire volume of moderator graphite contained in the fission chamber. With out online refueling, the SMMSR is limited to the fissile inventory contained within the fixed volume of fuel salt contained within the primary system. The core contains ~8.4 cubic meters of fuel salt, whereas the entire primary inventory is 16.8 cubic meters. The primary system inventory excluding that amount of fuel located within the core is about 50% that of the core. Therefore the achievable burnup of a given fuel salt loading is the burnup achieved by the depletion calculation multiplied by 2. A KENO

VI depletion was performed on the quarter core model to determine this burn up limitation and the results are plotted in

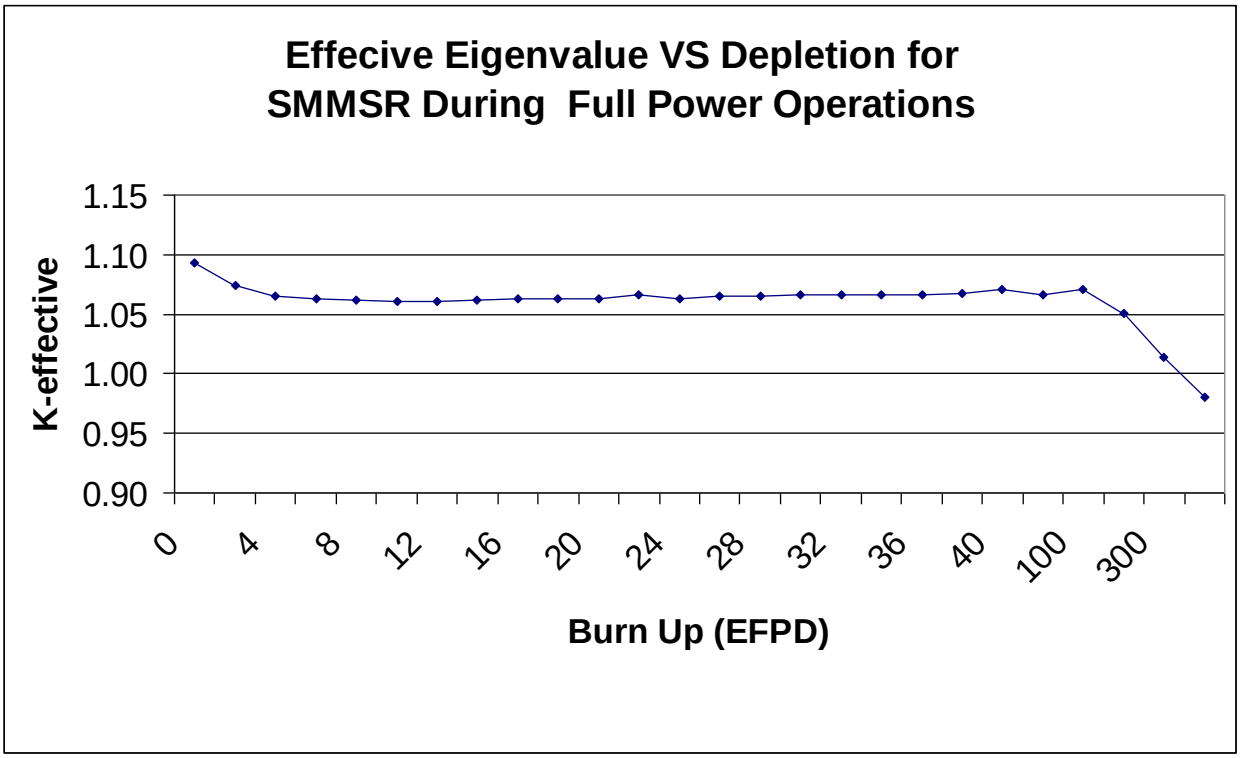

Figure 8. The actual time step eigenvalue data is multiplied by 2 for these results. At 240 MWt, the SMMSR with 2.5 mole fraction of 5 w/o UF_4 is capable of achieving ~341 Effective Full Power Days (EFPD) of operation before dropping below an effective eigenvalue of 1.0. Actual leakage conditions were modeled around the outer periphery and the top and bottom of the 3D model. The operational plan for the SMMSR is that a relatively small but constant fuel addition process will occur as the system is operating such that the number density of fissile material in the fuel salt remains adequate throughout core life to just overcome the negative reactivity induced by depletion and fission product build up within the primary fuel salt.

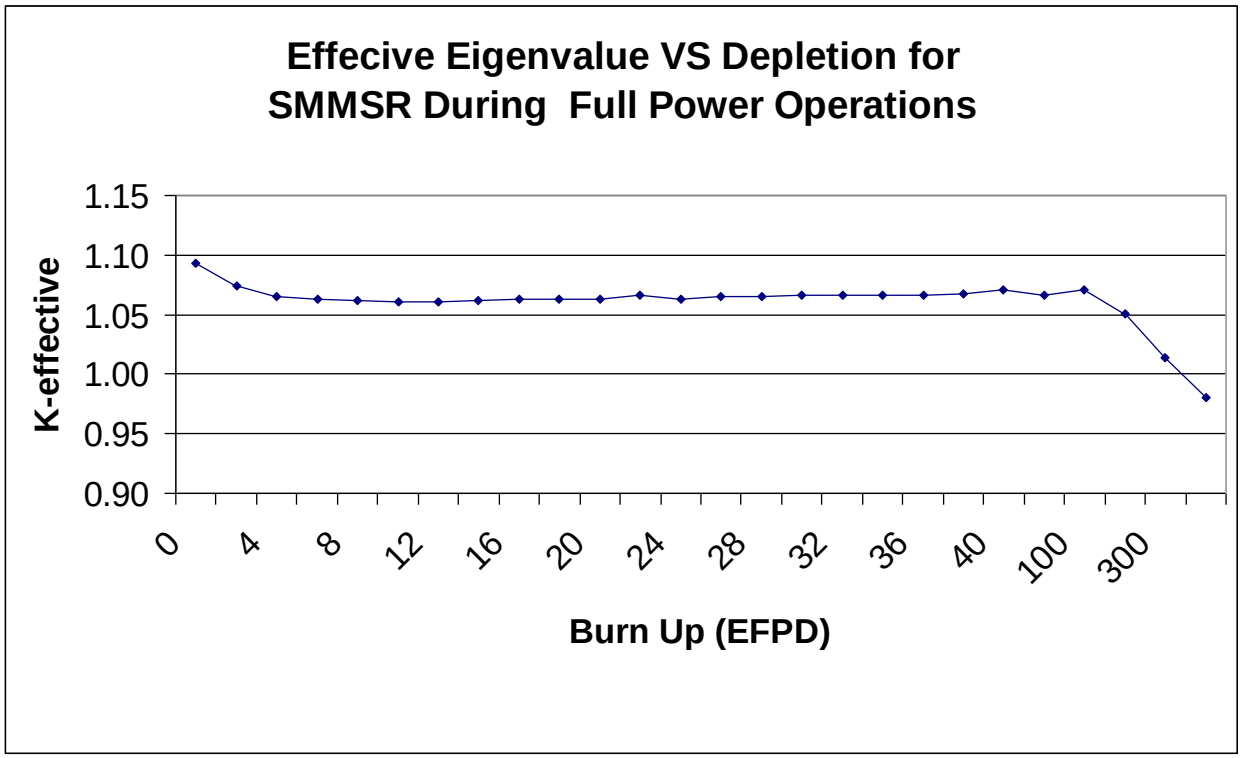

Figure 8: Effective Eigenvalue VS Burnup for Full Power Operations and No Fuel Addition

What can be observed from the results of the depletion analysis is that using UF_4 mole fraction manipulation as the mechanism of regulating primary coolant temperature will require very fine control in order to keep the temperature band reasonably small. For the first 8 days of full power operations, system reactivity swings by ~30 PCM before reaching an equilibrium Eigenvalue of ~1.06. After 8 EFPD and up to about 190 EFPD, system reactivity remains relatively constant. Then a noteworthy decline in system reactivity is observed from about 200 EFPD up to 340 EFPD where the system Eigenvalue drops to below 1.0. It is observed that initial start up will likely require reduced power operations with probably something less than a 2.5 mole fraction of UF_4 until the fission products burn into an equilibrium state. Even after the fission product equilibrium is achieved, it is anticipated that the system will regulate itself at the target 1000K with a smaller mole fraction than the initially proposed 2.5. With a mole fraction in excess of this value, the systems regulating temperature will start out being too high. At a 2.5 mole fraction and with a temperature coefficient of -3.4 PCM/K, the regulating temperature at initial start up would be in excess of 2400K. The start up concept discussed in **Section 6.2.1** states that UF_4 will be gradually added via continuous vapor feed into the fuel salt in order to start the system up. It is anticipated after seeing these results that the initial UF_4 mole fraction will be somewhat less than 2.5 in order to achieve the normal operating temperature of ~ 1000K. It may be necessary to engineer the SMMSR to be tolerant of a somewhat wide temperature band of operation in that any small reactivity effect will impact the regulating temperature of the system. The regulating temperature could vary by perhaps 50 to 100 K during steady state operations between fuel additions. The most encouraging observation of the depletion analysis is the relatively flat reactivity behavior of the SMMSR over a range of approximately 180 EFPD of operation. This suggests that fuel addition can be performed as a small batch add occurring possibly only about every 6 months or so, depending upon the range of operating temperatures that the system is engineered to tolerate. It is also observed that the KENO VI depletion analysis did not remove any gaseous fission products during the depletion calculation. The SMMSR has the built in ability to purge these gasses, like xenon, during fuel salt circulation and the reactivity benefit will lengthen the cycle time needed between fuel batch additions.

3.2.4 Primary to Secondary Heat Exchanger

3.2.4.1 Introduction

The primary heat exchanger selected for this project design is a compact version, constructed of liquid-silicon-impregnated (LSI) carbon-carbon composites. Compact carbon heat exchangers are in the advanced design and testing stages with research funded by the Department of Energy (**Reference 3**). The goal is to develop a compact efficient high temperature heat exchanger compatible with a variety of heat transfer fluids, one of which is molten salt. It is expected that this new design could be available for commercial production coinciding with the design, testing, licensing and deployment of a Generation IV Reactor for use in a remote location or in an emerging country. In case of an unexpected delay or unanticipated design flaw in the carbon heat exchanger, printed circuit heat exchangers (PCHE) are already used in industrial applications and are readily available based on customer specified design criteria and would be the second choice for the primary heat exchanger. A custom designed PCHE could be requested from one of the production companies built from a molten salt compatible metal, such as Hastelloy-N.

LSI carbon composites are capable of operating in the temperature range of 1000K to 1370K with both high-pressure helium and molten fluoride salts. LSI composites have several attractive features, including the ability to maintain nearly full mechanical strength to temperatures approaching 1700K, the capability for simple forming and machining with the use of inexpensive and commercially available fabrication materials. The fabrication of highly complex geometric shapes is possible to form system components. LSI carbon composite density is in the range of 2.0 g/cm^3 with a thermal conductivity of 690 W/m-K. The compact carbon heat exchanger is also compatible with the fuel and coolant salts selected for this project. **Table 6** demonstrates compatibility with different coolants. Also important, carbon has negligible solubility in molten salts and is resistant to fouling from noble metal precipitates.

Table 6: Compatibility of LSI Composites with Different Coolants [4]

Application	Molten Salt	High Pressure Helium	S-I Process Fluids
Intermediate molten salt loop for near term nuclear hydrogen	X	X	X
*AHTR (Hydrogen Production)	X		X
*ATHR (Electricity Production)	X	X	
Molten Salt Reactor	X	X	
Fusion Chamber Coolant (Electricity Production)	X	X	
X – signifies compatibility between the fluid and the Application			
*Advanced High Temperature Reactor			

Compact plate-type heat exchangers, like the LSI composite design, furnish very high surface area to volume ratios, require small fluid inventories and decreased mass flow rates. Current industrial machining methods allow the fabrication of carbon/carbon plates from a few to several millimeters thick from chopped carbon fiber material. The alternating counter flow channels of the resulting LSI heat exchangers look like those shown in **Figure 9** below. The figure shows alternating molten fuel salt (Blue) and coolant salt (Red) flow channels. Dark bands at the top of each fin indicate the location of reaction-bonded joints between each plate (Source: **Reference 3**).

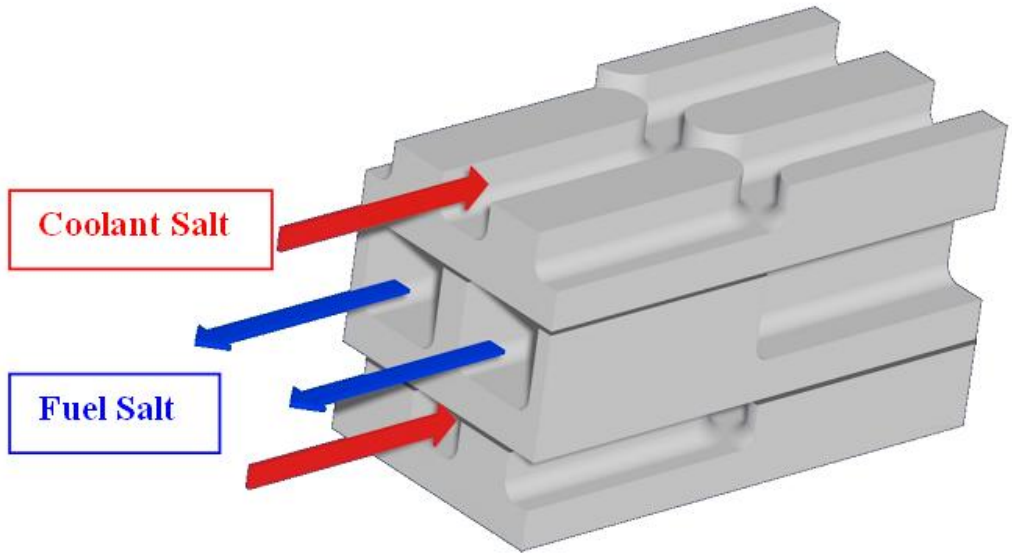

Figure 9: Cut Away View of LSI Heat Exchanger

3.2.4.2 Design

The FLIBE physical properties given in **Table 3** and **Table 7** were used in the development of this design.

Table 7: Physical Properties of FLIBE-UF4 Fuel and FLIBE Coolant Salts

Material	ρC_p (kJ/ m^3-K)	Heat Transfer Coefficient (W/m^2-K)	ν x 10^6 (m^2/s)
Li_2BeF_4	4540	~6000	2.9
$Li_2BeF_2UF_4$	5040	~6000	~2.9

Table 8: Primary Heat Exchanger Design Parameters

Design Parameter	Value	Units
Thermal Power	240	MW
Hot Side (FLIBE Fuel Salt) T_{in}/T_{out}	1000 / 800	K
Cold Side (FLIBE Salt) T_{in}/T_{out}	780 / 980	K
ΔT	20	K
Fin Heights Hot/Cold	2.0 / 1.0	millimeters
Flow Path Length	1.05	meters
Pressure Loss Hot/Cold	7.56 / 15	kilopascals

The primary heat exchanger designed for this project has vertical fin heights of 2 mm for the hot side (FLIBE molten fuel salt) and 1 mm for the cold side (FLIBE molten salt) with the hot and cold fluid in a counter flow alternating plate configuration. The hot side entry temperature is 1000K with an exit temperature of 800K. The cold side has an entrance temperature of 780K with an exit temperature of 980K, which results in a ΔT of 20K. The conceptual design parameters are given in **Table 8**. The calculated mass flow rate of approximately 500 kg/s through both the hot and cold side of the primary heat exchanger favorably parallels requirements for mass flow rates through the reactor core design. The overall size requirements for the primary heat exchanger are 1.05 flow length (m) x 2.5 height (m) x 3.8 depth (m). This gives a total active volume of 10 m^3 resulting in a thermal density of 24.8 MW/ m^3. The carbon core is encapsulated in a 2 cm thick Hastelloy-N shell to accommodate distribution headers and attachment to the primary piping. The calculated total mass is approximately ~15,700 kg. The primary heat exchanger size and weight accommodate the original requirements of the overall plant design for

compactness and transportability. The distribution header at the top of the heat exchanger has many functions in the SMMSR primary system. It serves as a point of fission product gas removal from the primary loop. It is the entry point for fuel addition via the fluorination system, and for dilution via secondary FLIBE salt addition. And it has an oversized shell to serve as the surge volume for thermal expansion and level variation of the fuel salt. From the density function in Table 3, the expansion volume necessary for the fuel salt can be computed. For a fluid temperature variation from just above freezing (736K) to just below boiling (1700K), and with a primary volume of ~17 cubic meters, the surge tank must be able to hold an expansion volume of ~1.5 cubic meters.

3.2.5 Core Dump Tank

The SMMSR primary system is equipped with an emergency core dump tank which is located immediately beneath the moderator chamber (see **Figure 2**). It is connected to the core vessel via a 1 meter diameter down pipe which contains a freeze plug or more commonly called a freeze valve. This plug is formed in the down pipe by an integral heat exchanger which freezes the FliBe+UF_4 fuel salt in the pipe via active cooling. This cooling is accomplished with a series of small diameter tubes passing through the down pipe which have cool helium gas passing through them. As long as the active cooling is functioning, the freeze plug remains frozen. Upon an over temperature condition, or a loss of active cooling, the frozen fuel salt will absorb heat from the above fluid and melt, thus allowing the primary inventory to drain via gravity into the core emergency dump tank.

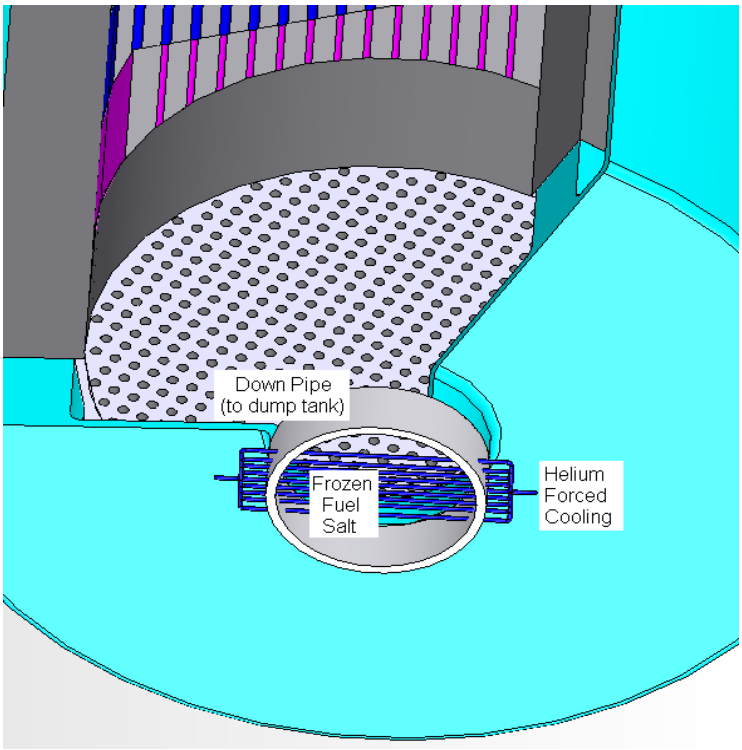

Figure 10: Freeze Valve Cooler and Down Pipe

The core emergency dump tank takes up the entire volume underneath the reactor vessel up to 2 meters from the floor to create a tank volume of 4.7 meters by 4.7 meters by 2 meters high, or 44 cubic meters in volume. Since the fuel salt volume in the primary system at full temperature occupies ~17 cubic meters, this leaves over half of the volume in the tank unoccupied to allow for thermal expansion, fission product gas release, and shut down reactivity materials. The tank could contain several cubic meters of un-enriched FliBe salt in solid form such that the high number density of thermal neutron absorbing lithium 6 would act as a reactivity hold down, and the frozen salt would add thermal inertia in the form of absorbing

latent heat of fusion from the high temperature liquid fuel salt. The freeze valve and cooler are illustrated in **Figure 10**.

3.2.6 Upper Biological Shield Assembly

As was stated in Section 3.2.1, the primary containment structure has a removable upper shadow biological shield. This shield is composed of lead for gamma dissipation, hydrogenous material for neutron thermalization, and borated concrete for thermal neutron absorption. It is shaped as a partial inverted cone so as to provide adequate line of site shielding from the extremities of the primary containment module to the surface. It is sized in such a manner as to provide maximum necessary shield protection from any above grade angle from direct or scatter radiation emanating from any primary components. The material layout is shown in **Figure 11**. The arrangement allows for the hydrogenous material before the borated concrete so as to thermalize leaking neutrons and increase the probability that they will be captured in the boron, and to minimize gamma embrittlement of the hydrogenous material.

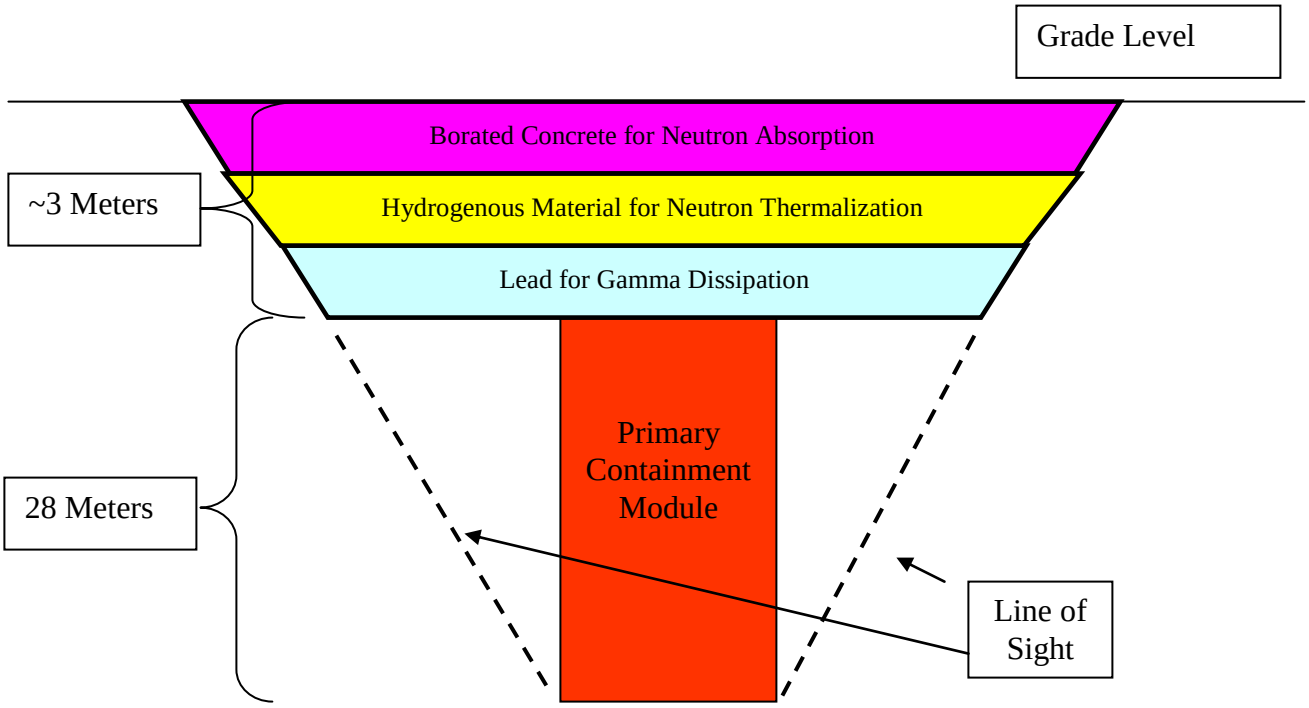

Figure 11: Biological Shadow Shield Layout and Material Composition

3.2.7 Other miscellaneous

The UF_6 to UF_4 fuel fluorination and addition system is also located within the primary containment module. It is positioned above the inlet box of the primary to secondary heat exchanger. It is connected to the upper heat exchanger inlet box for fuel salt addition.

3.3 System Operation Description

3.3.1.1 Normal Full Power Operation

The SMMSR is designed to operate in steady state and load following mode as an autonomous critical system in that no active control devices such as control rods or moving reflectors are necessary to regulate the core thermal power output or temperature rise. This is accomplished by taking advantage of the unique features that the liquid fuel form makes available. Operation of the moderator chamber was

explained in **3.2.3**. The primary system operation is an extension of the moderator chamber operation as follows. Under normal demand, the primary to secondary heat exchanger has heat being transferred from the primary salt to the secondary salt as the power cycle draws heat for power production from the secondary loop. The fuel salt leaves the heat exchanger because, by virtue of the fact that it is cooler than the hot leg fuel salt, its density is greater and the differential head creates the driving head for the natural circulation within the loop. The cool fuel salt enters the moderator chamber and induces a local negative net reactivity. The energy which is generated is deposited into the fuel salt and its density decreases such that each axial region of the core will achieve only the designed temperature increase as determined by **Table 5**. The temperature of the outgoing fuel salt increases and the reduction in density further enhances the head differential for natural circulation. The hot salt enters the heat exchanger and energy is drawn off by the secondary fluid.

3.3.1.2 Accident Scenarios

By using a liquid fuel system, there is no value for a coolant void coefficient. Since the fuel material is the coolant material, a reduction in coolant density (voiding) reduces the critical mass of the fixed volume and shuts down the chain reaction. There is also no such concept as a departure from nucleate boiling because of a lack of a fuel to coolant physical interface region. Since the fuel salt is already in a liquid state, there is no approach to centerline fuel melt, or cladding failure temperature limit. In a molten fuel system, these safety parameters simply do not exist, thus making the SMMSR system inherently safe and simple to operate.

There are some theoretically possible accident scenarios which deserve mention here. It is possible that the UF_4 addition process could malfunction in such a way as to add too much fuel to the system. Since the number density of fissile material is the key variable in how the SMMSR maintains the fuel salt at the regulated temperature, such a scenario would cause the system temperature to increase. The safety mechanism built into the SMMSR for mitigating such an accident is two fold in nature. First, the operators or an automated system could introduce additional base solvent FliBe from the secondary loop into the primary so as to dilute the fuel salt and reduce the mole fraction of UF4. If this action is insufficient or is not taken, the core safety freeze valve, or dump valve, will melt and release the primary fuel salt inventory into the safety dump tank. A more detailed discussion of this system is located in **3.2.5**.

Another potential problem for a load following system is the possibility that more power could be drawn off of the system than that which it is designed to produce. The SMMSR as proposed is rated at a maximum steady state output of 240 megawatts thermal output. Should the power cycle demand more than this rated power, automatic trip functions should reduce the load and keep the system from overpowering. In such a case as the system does not trip, the primary systems physical response would tend to drive power down and lead to a safe system shut down as follows. As the power drawn exceeds 240 megawatts, the differential temperature across the core would increase above the normal design value of 200K. The cold leg temperature is maintained at above 820K, and as the core delta-T increases, the cold leg temperature would drop. The freezing temperature of the fuel salt as stated in **Table 3** is 736K. As the temperature of the cold leg approaches this value, the fluid's viscosity will decrease and add to the pressure drop in the primary loop. As the system is using natural circulation, an increased pressure drop will reduce the flow of the fuel salt through the primary loop. As the fuel salt flow rate decreases, so to will the power generated in the fission chamber. But without an associated decrease in power cycle demand, the cold leg will continue to drop in temperature until the salt begins to solidify. Such obstruction in flow will continue to drive the power production downward until the primary circuit fuel salt flow comes to a complete stop.

4.0 Secondary System

4.1 System Overview

The secondary system or intermediate loop is intended to absorb heat from the molten fuel salt at the primary heat exchanger and transport it to the power conversion system through the secondary heat exchangers. In addition to the primary function of heat transport, the secondary system also serves as an important barrier to isolate the radioactive primary circuit from the power conversion system. The fluid selected for this function is identical to the fuel salt without the addition of uranium tetrafluoride (UF_4). This coolant was selected because of superior heat transfer qualities and a very low vapor pressure. Also included in the secondary system are the components that are required to circulate, cool, heat, contain and control molten salt up to the primary heat exchanger exit temperature of 980K. The hardware required for the secondary system operation includes heat exchangers, pumps and piping along with expansion tanks, storage tanks, valves, instruments for sensing and adjusting operating conditions and heater banks for system heat up and initialization. The critical components required for the secondary system are described in **Section 4.2**.

4.2 System Components

Lithium beryllium fluoride, Li_2BeF_4 (66-34 FliBe), is selected as the secondary coolant because it has excellent heat transfer characteristics and is completely compatible with the fuel salt, $Li_2BeF_4UF_4$. Under any anticipated condition or event, such as a primary to secondary system leak in the heat exchanger, or a need to dilute the primary fuel salt due to an over feeding of fuel, the secondary salt can serve as a standby source of fuel salt dilution material or as a coolant make up reserve. The primary heat exchanger is the location where the two salts are adjacent in the system, separated by only a millimeter of the carbon-carbon composite structure. Precipitation of fissile material would not occur nor would reaction product gases evolve with mixing of the two salts. No reactions occur between the two salts, other than mixing of two miscible liquids. Leakage of the coolant salt into fuel salt only dilutes the uranium that could ultimately lead to safe reactor shutdown resulting from a non-critical fuel configuration. No nuclear poisons would be added to the fuel salt and no purification or special processing would be required. Leakage of fuel salt into the secondary coolant loop would require shutdown and clean-up due to radiological contamination, but no precipitation or other reactions would occur. It is advantageous to maintain a slight pressure differential so that leakage in most cases would be predominantly from the secondary coolant into the fuel. One disadvantage of Li_2BeF_4 coolant salt is that the lithium needs to be enriched to greater than 99.99% lithium 7 to prevent ruining the fuel salt by the addition of lithium 6 in case coolant leaked into the primary system. The physical properties of both the fuel salt and coolant salt are given in **Table 3**.

4.2.1 Secondary to Helium Heat Exchanger

The heat exchanger selected for the secondary system is also a compact heat exchanger type or commonly referred to as a Printed Circuit Heat Exchanger (PCHE). These types of heat exchangers are already in use in industrial environments and are available from manufacturers based on customer desired operating parameters. PCHEs offer high compactness and high efficiency which saves in both costs and weight. PCHEs provide high surface area to volume ratios and can also withstand pressures up to 50 MPa, which is much greater than the design pressure for the power conversion system.

Helium is the transfer coolant used for the power conversion system and circulates on the cold side of the secondary heat exchanger, where it absorbs heat from the coolant salt and delivers it to the Brayton cycle turbines. Thermal densities for salt to helium heat exchangers are in the range of 80 to 120 MW/m^3. For this design project, three compact heat exchangers are used of approximately 1 m^3 each to transfer 240 MW of thermal energy to the power conversion system. Three are used sequentially for increased efficiency. The helium is heated to its peak temperature of approximately 960K and then flows through a

turbine to reduce its pressure by one third. It then flows through the second heat exchanger to return to its peak temperature, then through the second turbine to reduce its pressure by another third. It then flows through the third heat exchanger returning to its peak temperature and through the last turbine. The helium returns to the first of the secondary heat exchangers after exiting the power conversion system. Design parameters are given in Table 9Table 9.

Table 9: Secondary Heat Exchanger Design Parameters

Design Parameter	Value	Units
Thermal Power	240	MW
Hot Side (FLIBE Salt) T_{in}/T_{out}	980 / 780	K
Cold Side (FLIBE Salt) T_{in}/T_{out}	760 / 960	K
ΔT	20	K
Fin Heights Hot/Cold	1.0 / 2.0	millimeters
Flow Path Length	0.49 to 0.33	meters
Pressure Loss Hot/Cold (max)	186 / 34	kilopascals

A cross sectional view of a compact heat exchanger constructed with 0.025" channel walls is shown in **Figure 12** and an illustration of the alternating counter flow arrangement of a compact heat exchanger is shown in **Figure 13**.

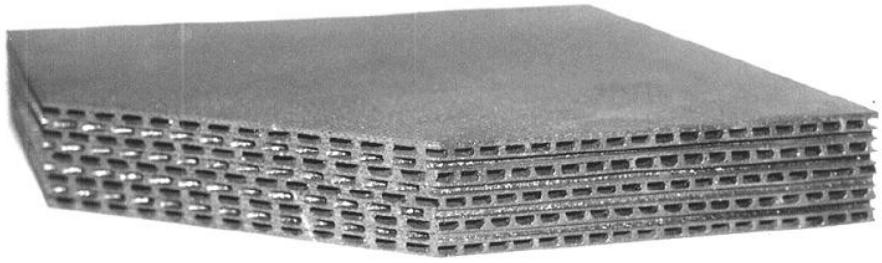

Figure 12: Compact C/SiC Cross-Flow Heat Exchanger

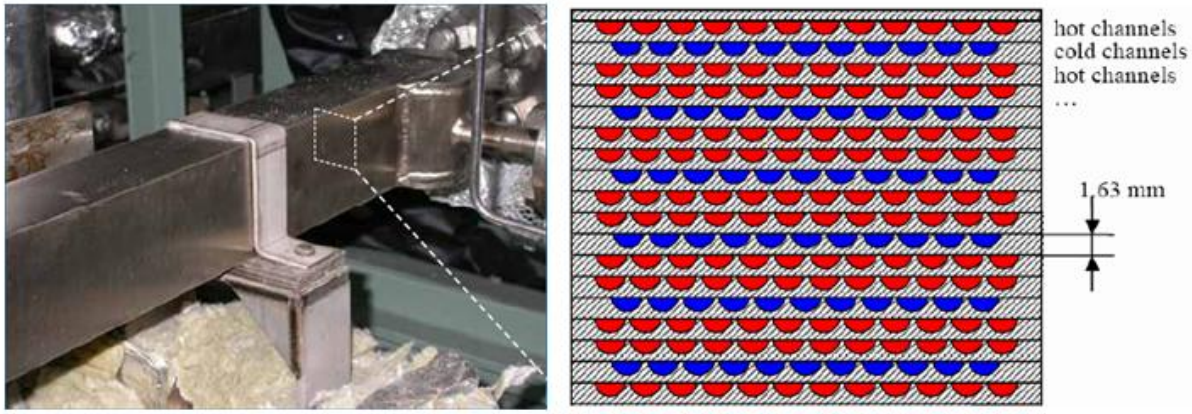

Figure 13: Compact Alternating Plate Counter Flow Heat Exchanger

Key thermo-physical properties of FliBe coolant salt and helium are given in **Table 10.**

Table 10: Physical properties of FliBe Coolant Salt and Helium

Property	Helium	LiF[66]-BeF2[34]
Melting Point (K / C)	1 / -272	733 / 459
Boiling Point (K / C)	4 / -269	1703 / 1430
Density (kg/m^3) @ 1089 K	3.8 (@ 7.06 MPa)	1940

Thermal Expansion (per K)	1.9×10^{-4}	4.88×10^{-4}
Specific Heat (kjoule / kg-K)	5.2	2.34
ρC_p (kJ/ m^3-K)	20	4540
Heat transfer Coefficient (Watt / m^2-K)	0.29	1.0
$\nu \times 10^6$ (m^2/s)	11.0	2.9

4.2.2 Secondary Piping

The secondary piping and components that come into contact with the molten salt are constructed of Hastelloy-N. The design pressure for the secondary side is slightly above the primary loop so that a leak at the primary heat exchanger would be from the secondary to primary side. This is a safety feature to contain the radioactive fuel salt and result in reactor shutdown if a major leak occurred at the primary heat exchanger. In the case of a severe heat exchanger leak, the fuel salt would be diluted to a point below criticality resulting in shutdown. The primary loop operates at almost atmospheric pressure or 0.1 MPa. The secondary salt is circulating at a mass flow rate of 500 kg/s. The diameter of the secondary piping is approximately 33 cm. These numbers mirror the design of the primary system flow for heat transport in the primary heat exchanger. To select the piping for the secondary system, a conservative design stress pressure of 5 MPa is allowed. It is also conservatively assumed that the system pressure is 0.5 MPa or 5 times the primary system pressure. Using **Equation 1** which is repeated here as **Equation 7**:

Equation 7: Hoop Stress

$$\sigma_h = (p \cdot r)/t$$

where σ_h=hoop stress, p=pressure in pipe, r=radius of pipe, t=thickness of pipe or 5 MPa = (0.4 MPa · 0.165)/t and t= approximately 1.3 centimeters or 0.5" thick. The longitudinal stress would be roughly half of the hoop stress, so Hastelloy-N piping of 1.27 cm (0.5 inch) is sufficient when stress is limited to 5 MPa. Hastelloy-N can withstand up to 11 MPa, so this is conservative by a factor of two. The selection would also be seamless piping except where joined to other components in the system. The piping would also be covered with insulation to minimize environmental losses.

4.2.3 Secondary Salt Circulating Pump

The pump for circulating the molten salt would be installed before the inlet to the primary heat exchanger to maintain the safety designed positive pressure over the primary side of the heat exchanger. Centrifugal pumps have been designed to operate at the high temperatures of molten salt and tolerate a molten salt environment. The design pressure for the pump is 0.5 MPa. The pump consists of a pressure vessel, clutch and bearing boxes and the electric motor. A picture of a molten salt pump of this design is given in **Figure 14**.

Figure 14: Secondary Salt Circulating Pump

4.3 System Operation Description

The initial start up of the secondary system would most likely occur before the primary system heat up and also probably include some kind of pressurizing and purging as heat up begins to ensure moisture and oxygen are removed from the system. The electrical bank or pressurized gas heaters located strategically throughout the secondary system would provide the thermal energy for startup. As the molten salt is heated, the pump is engaged and circulates the fluid. The heaters or the circulating pump can be used to maintain the desired operating temperature until the primary loop and core are operational. Concurrently, helium would be circulated to remove heat from the intermediate loop as the plant starts operation. Installed instrumentation monitors pressure, flow and temperature and provides feed back to the system equipment to maintain the desired operating parameters.

5.0 Power Conversion System

5.1 System Overview

The power conversion system is an essential element in any nuclear reactor design, converting the high-temperature thermal energy generated by the reactor into usable shaft work and ultimately into electrical energy for further distribution. The efficiency of the power conversion system is broadly limited by thermodynamic considerations, such as the average temperature at which thermal energy is added to and rejected from the conversion system, and efficiencies in the components themselves.

For a number of reasons, a helium gas-turbine power conversion system, often referred to as a Brayton cycle, was chosen as the power conversion system for the reactor. Unlike conventional gas-turbines, which use combustion as a heat source and operate on an open-cycle with air as the working fluid, this cycle utilizes nuclear heat addition and a closed-cycle with helium as the working fluid.

Helium gas turbines of this configuration are not currently in use in industry today, primarily due to lack of a suitable non-combustion heat source. Nevertheless, the thermodynamic and practical advantages of the closed-cycle helium gas turbine are so great that they are being considered for a variety of advanced reactor concepts, such as sodium-cooled fast reactors and very-high temperature gas-cooled reactors.

There are subtle differences between how a helium-Brayton cycle can be implemented to maximum advantage in each of these reactor types, but there are overall similarities that can be observed.

In each case, the helium gas is compressed at relatively low temperatures and at the minimum pressure of the cycle. Compression is executed at low temperature to minimize the work input to the gas during compression. Nevertheless, compression consumes roughly half of the overall shaft work generated by the cycle. After compression, which may take place in one stage or over several stages separated by intercooling, the gas flows to a regenerator. The regenerator is essentially a counter-current heat exchanger. In one channel of the regenerator the high-pressure gas from the compressor exhaust is heated to much higher temperatures by the flowing, low-pressure exhaust of the last turbine stage. Regeneration is a feature commonly found in high-performance closed-cycle gas turbines and improves the thermodynamic efficiency of the system markedly.

After exiting the regenerator at a much higher temperature than the entrance, the high-pressure gas is then heated to its maximum temperature. In this reactor design, this heating is achieved by passage through a counter flow heat exchanger where hot fluoride coolant salt, used to cool the reactor, is used to heat the helium to its maximum cycle temperature. In other nuclear gas-turbine concepts the gas might be directly heated in the reactor vessel itself. After being heated, the gas is then expanded through a turbine, generating shaft work. A substantial portion of this shaft work is used to drive the compressor (roughly half) but the remainder can be used to drive an electrical generator, where shaft work is converted into electrical energy at high efficiency (>95%).

Table 11: Power Conversion System Parameters

Parameter	Value	Units
Design Electrical Power	100	MW
Electrical Generator Efficiency	95%	
Thermal Power Addition	224	MW
Thermal Power Rejection	120	MW
Cycle Efficiency	44.8%	
Net Work	1.3	MW/kg/s
Helium Mass Flow Rate	81	kg/s
Coolant Salt (2LiF-BeF2) Mass Flow Rate	538	kg/s
System Description	Triple-reheat closed-helium cycle	
Compressor Inlet Temperature	300	K
Turbine Inlet Temperature	960	K
Gas Heater Inlet Temperature	760	K
Total Compression Ratio	5.52	
Compressor Inlet Pressure	2.0	MPa
Turbine Efficiency	92%	
Compressor Efficiency	88%	
ΔT across Regenerator	25	K
Pressure Losses	1%	per 100 K of heat exchange
Hi/Int/Low-pressure Gas Heater Pressure	10.5/5.9/3.3	MPa
Hi/Int/Low-Pressure Turbine Power	75/75/64	MW
Hi/Int/Low-Pressure Compressor Power	37/37/38	MW
Cycle Net Power	103	MW

After passage through the turbine, the gas has lost a great deal of enthalpy. Depending on the design of the cycle, the gas might be reheated again and pass through another stage of turbine expansion, or it might

pass directly into the regenerator. Entering the regenerator, the low-pressure (but still rather high-temperature) gas is used to "pre-heat" the incoming high-pressure stream to improve thermodynamic efficiency.

Upon exiting the low-pressure side of the regenerator, the gas must be further cooled by contact with an external cooling fluid before reaching the lowest temperature of the cycle and entering the compressor. This cooling fluid might be ambient air or water. Air has the profound advantage of being available as a heat sink no matter where the reactor might be operated, but is disadvantaged in the large volumetric flow rates and large heat exchange surface required for cooling. A dense fluid like water is a much better cooling medium, but depending on the application, water might be in short supply. Another consideration might involve using cooling water for desalination purposes, if the reactor is located near to a body of salty water.

The design of the thermodynamic cycle has profound ramifications for the overall reactor design, and the reactor design sets constraints on the thermodynamic cycle design. For a reactor employing a liquid fluoride salt as a cooling medium, the high temperature capability of the salt allows very impressive thermodynamic conversion efficiencies to be readily achieved, on the order of 40-50%, depending on specifics of cycle design. The fact that the heating fluid is a fluid, rather than a fixed core (like a gas-cooled reactor) also affords the possibility of multiple stages of heating, rather than a single heating (and expansion) stage. Reheating leads to greater work extraction per unit mass of the helium working fluid. This in turn reduces the flow rate of helium required and reduces the size of the regenerator, which is typically the largest heat exchanger in the system.

The decision to use a liquid fluoride salt also levies constraints on the cycle design as well, the most pronounced of which is the need to keep the minimum temperature of heat addition in the cycle above the freezing point (liquidus) of the salt. Typical liquidus temperatures in the fluoride salt are such that a regenerated cycle is practically a requirement for any practical machine.

To design the thermodynamic cycle for this reactor, it is necessary to recognize some of these unique design considerations. Typically, a Brayton cycle designer begins with an overall concept of the cycle based on the compressor inlet temperature (the minimum temperature of the cycle), the turbine inlet temperature (the maximum temperature of the cycle) and the overall compression ratio of the cycle (the ratio between the compressor outlet pressure and the compressor inlet pressure).

For this design, the requirement to keep heat addition above the liquidus temperature of the salts led to a modification of design strategy. Instead of specifying turbine inlet temperature and compression ratio, the gas heater inlet temperatures and heater outlet temperatures were specified, as well as the compressor inlet temperature.

The rationale for this was a recognition that the gas heater was the basic thermal interface between the reactor and the power conversion system, and that the specification of these two temperatures essentially came from the liquidus temperature on the low end (plus whatever thermal margin was deemed prudent) and the core exit temperature on the high end, which is a basic design input.

By specifying heater inlet and outlet temperatures, the pressure ratio for the turbine can be computed, given the adiabatic efficiency of the turbine. It may seem counterintuitive, but specifying the gas heater inlet and outlet temperatures essentially fixes the turbine pressure ratio. If multiple stages of heating and expansion are employed, then the overall compression ratio can be computed by accounting for pressure drops in gas heater, the regenerator, and the gas coolers. With the overall compression ratio computed, the stages and pressure ratios of the compression system can be calculated.

Assuming that heater inlet temperature represents a thermal constraint fixed by the liquidus temperatures of the coolant and core salts, increasing the core exit temperature has a pronounced effect on the power generated by each unit of gas flow, and a modest effect on thermodynamic cycle efficiency. There is a definite incentive to pursue higher core exit temperatures (which map directly into heater outlet temperature) but as we have mentioned in the core design section, this has a significant effect on allowable core power density because of the constraint of graphite lifetime.

Therefore it was necessary at a very early stage to integrate the power conversion system modeling tool into the overall reactor design. Higher PCS efficiencies lead to smaller thermal requirements for the reactor when the electrical output is a fixed 100 MWe. But in this design, higher PCS efficiencies driven by higher core outlet temperatures had the unfortunate effect of lowering allowable core power density because of constraints on graphite lifetime. Therefore, it was expedient to pursue all solutions for increasing cycle efficiency without increasing core outlet temperature.

As was previously mentioned, one of the most basic of these cycle improvements was the use of regeneration in the Brayton cycle. Regeneration markedly increased the temperatures at which heat was added to the reactor and essentially made it possible to enforce the liquidus thermal constraint. Another cycle improvement was the extensive use of intercooling in the compression system. Intercooling kept the overall temperature of the fluid during compression down, and reduced the amount of work needed to compress the gas. It may seem paradoxical that six compressors are doing less work than three or even one, but such is the nature of gas compression that multi-stage compression followed by intercooling can lead to significant performance improvement. The benefits of intercooling are also synergistic with the regeneration system, since the lower the compressor outlet temperature, the more enthalpy can be transferred in the regeneration system. Intercooling does increase the amount of cooling fluid required, however. Six stages of intercooling require approximately twice the flow of cooling fluid as three stages, even though the enthalpy rise across each cooler is cut in half.

The use of the cycle design tool allowed such system trades to be evaluated quickly and accurately. The final cycle design that was chosen for the power conversion system is shown in **Figure 15**, and is broadly bounded by the need to add heat to the gas at temperatures above the freezing point of the coolant salt, and the need to reject heat to the environment at as low a temperature as possible.

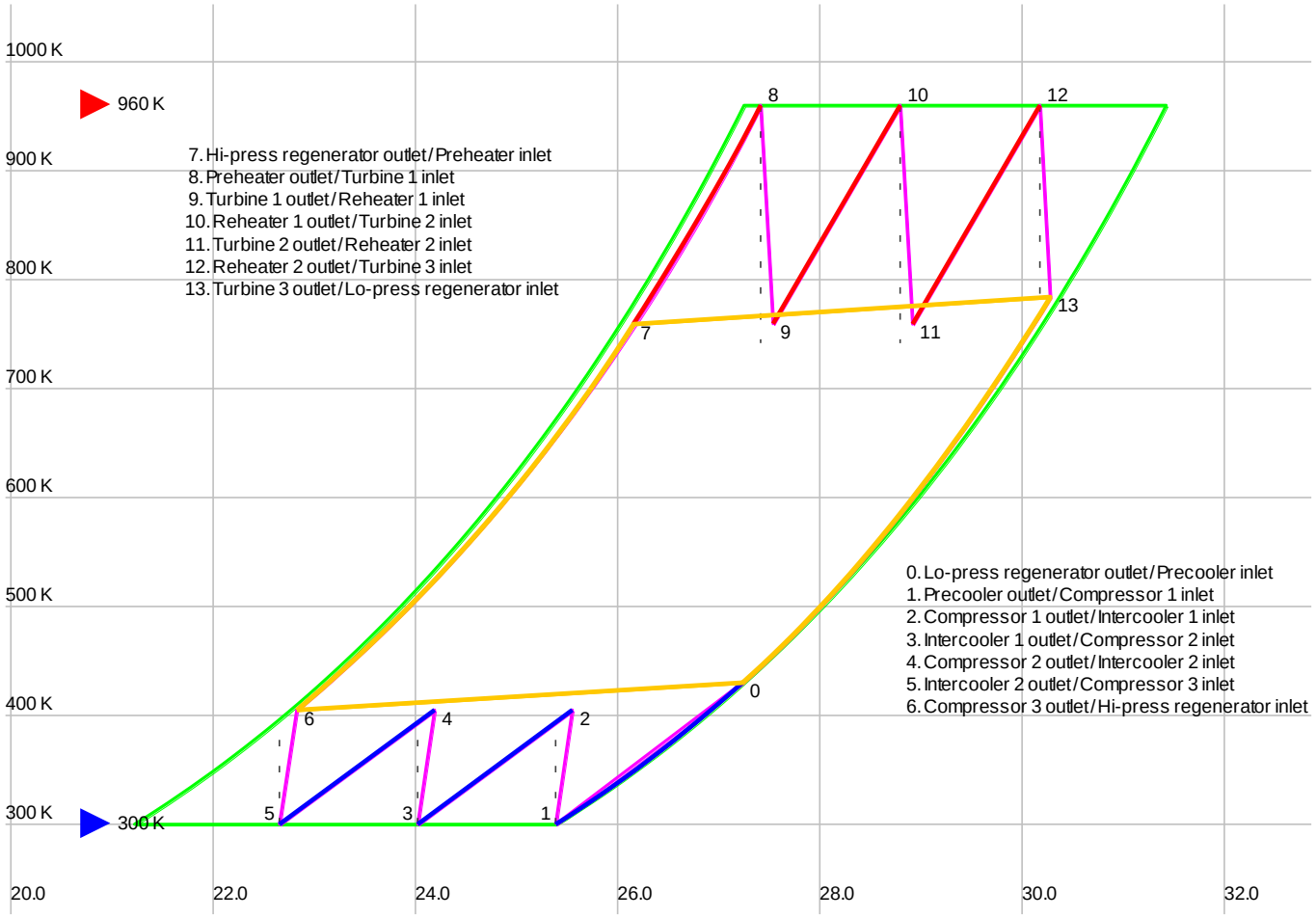

Figure 15: Temperature-Entropy Diagram of the Power Conversion System Cycle

5.2 Components

The power conversion system consists of three turbomachines and seven heat exchangers. Each of the three turbomachines has a turbine, compressor, and generator. The compressor and generator are mounted on opposite sides of the turbine and are both driven by the shaft power generated in the turbine, with the compressor consuming a little more than half of the shaft power produced by the generator.

Of the seven heat exchangers, three are heaters. The heaters are countercurrent printed circuit heat exchangers with coolant salt as the hot fluid (losing enthalpy) and helium as the cooling fluid (gaining enthalpy). The gas heaters precede each turbine stage and are the basic thermal communication between the reactor and the power conversion system.

Three of the heat exchangers are coolers. These are countercurrent printed circuit heat exchanger with helium as the hot fluid (losing enthalpy) and water or air as the cooling fluid (gaining enthalpy). The gas coolers precede each stage of compression and are the basic thermal communication between the reactor system and the outside environment.

The final heat exchanger is the regenerator. This is a gas/gas countercurrent printed heat exchanger with low-pressure helium, exiting the last stage of expansion, as the hot fluid and high-pressure helium, exiting the last stage of compression, as the cooling fluid. The regenerator is typically the largest of the heat exchangers in a fluid-heated, fluid-cooled closed-cycle helium gas turbine system, because both of its fluids are gases. The regenerator makes high-temperature heat addition and low-temperature heat

rejection possible by exchanging significant amounts of enthalpy between the high-pressure and low-pressure gas flows.

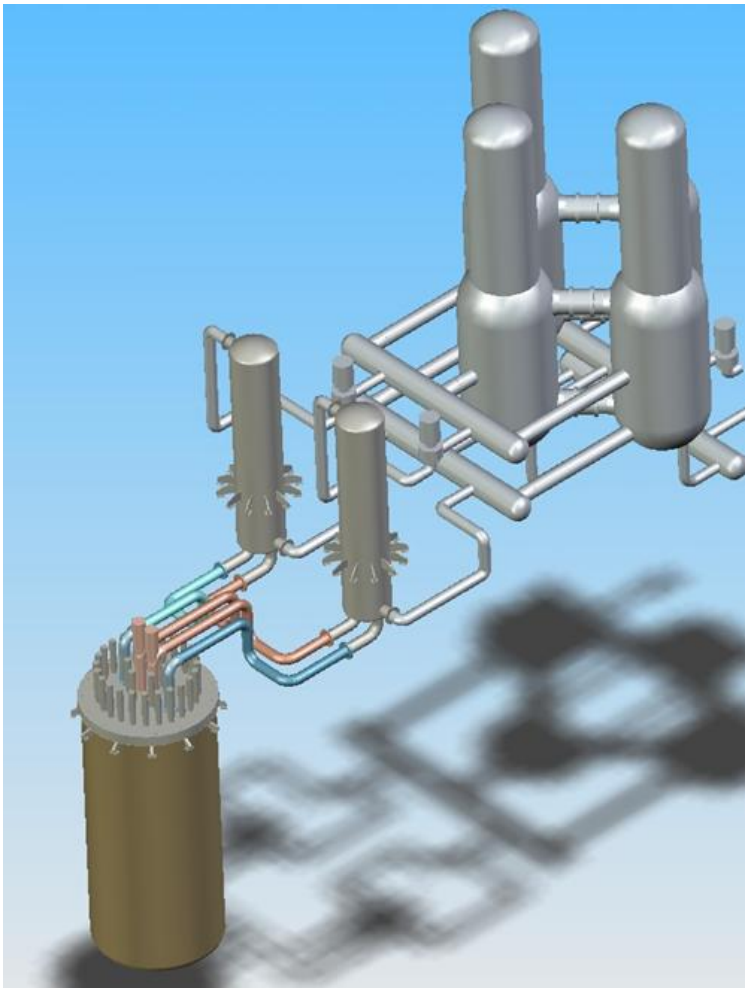

Figure 16: Illustration of Reheat Brayton Power Cycle

The overall system can be visualized in **Figure 16**, which is an image utilized from the Advanced High-Temperature Reactor program at ORNL. The AHTR also uses a liquid-fluoride salt as a core coolant medium and a triple-reheat closed-helium-cycle gas turbine power conversion system. The salient difference between the AHTR and this reactor design is that the AHTR uses solid fuel elements whereas this reactor uses a liquid-fluoride fuel. But both use a liquid-fluoride coolant salt and nearly identical power conversion systems.

In the illustration in **Figure 16**, one can see the reactor vessel at the lower left with hot coolant salt outlets and coolant salt inlets. In the upper left hand corner, the three turbomachines can be seen, oriented vertically and joined together by helium passages. On each turbomachine, the electrical generator is located on the top of the vertical stack. The regenerator is also joined in sequence with the turbomachines, transferring enthalpy from the hot, low-pressure exhaust of the final turbine to the high-pressure exhaust from the high-pressure compressor.

Within the turbomachines, cooled helium enters the compressor through an annular volute, and then passes through axial stages of the compressor. Alternating stages of rotors and stators increase the pressure, temperature, and enthalpy of the flow. After passing through the compression stages, the gas then enters an annular volute and is exhausted to an intercooling stage or to the high-pressure entrance of the regenerator.

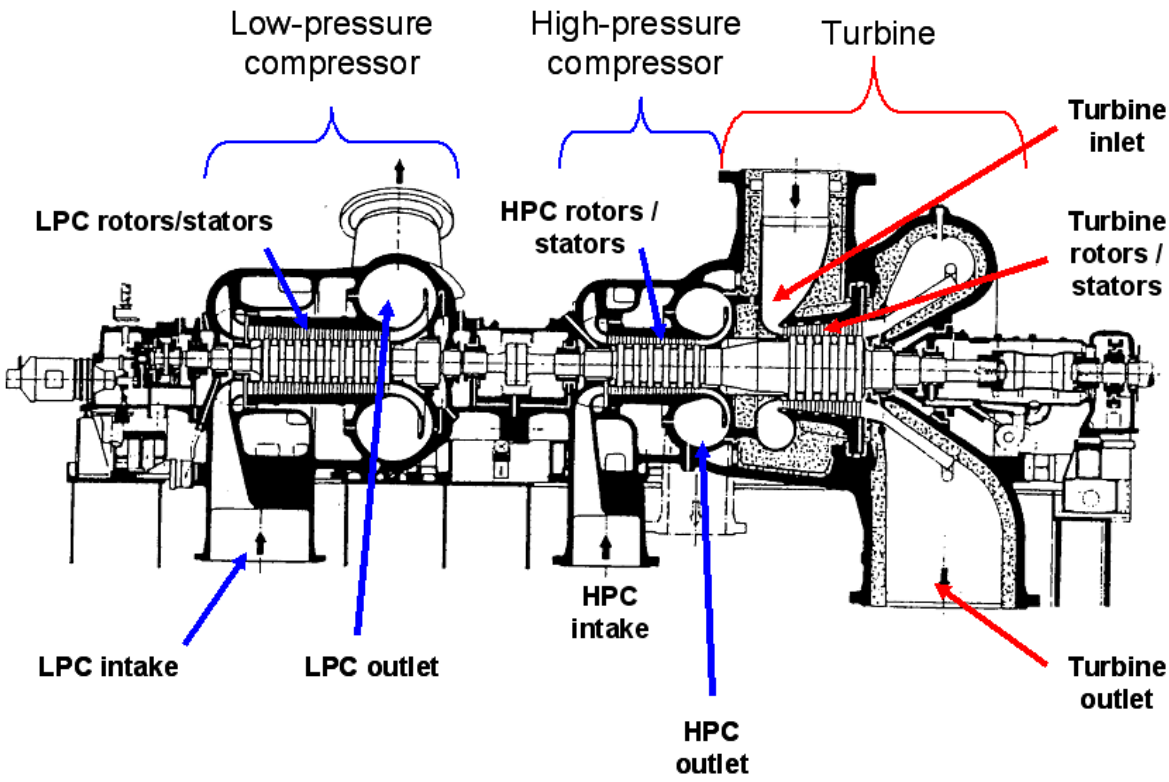

Figure 17: Integral Turbine and Compressor Unit for a Reheat Brayton Cycle

Heated helium, coming from the gas heater, enters the turbine in a similar manner through an annular volute. It then passes through similar rotor and stator stages of expansion, this time driving the stages and producing work. In the process, the gas is losing enthalpy, temperature, and pressure in a process as close to isentropic as can be achieved through proper design. Upon exiting the turbine through another volute, the gas either passes to another stage of heating or to the low-pressure entrance of the regenerator.

An example of the layout of the turbomachines is shown in **Figure 17**. This layout shows two compressors on the same shaft as the turbine. If two compressors were used per turbine, there would be six compressors overall in the system, along with six gas-cooling heat exchangers instead of three, but the required compression per turbomachine would be reduced by more than half, and the total heat rejection load would also decrease by more than half. It might seem paradoxical that more turbomachines and more heat exchangers would actually lead to less work consumption and less heat rejection, but this is because gas compression becomes more efficient the closer it can be brought to an isothermal condition. System complexity must be weighed against superior conversion efficiency.

5.3 System Operation Description

The electrical load of the power grid would communicate with the reactor through the power conversion system. At off-design conditions, a power demand less than the design value would result in less shaft power demand by the electrical generator. This is turn would manifest itself as a change in the pressure ratio across the turbine, which in turn would change the temperature difference across the gas heater. This change in temperature difference would then lead to a change in temperature difference in the primary salt, manifested as a hotter salt entering the core inlet. The negative temperature coefficient of reactivity would then reduce core power in accordance with a hotter core salt inlet temperature, leading to a reduction in power generation. Thus the core power generation would "follow" the load generated by the power conversion system naturally and without operator intervention.

6.0 System Life Cycle

6.1 Precommissioning

6.1.1 Module Construction

The SMMSR system is to be transported to the site in a modular fashion, with the primary, secondary, and power cycle components to be contained within individual modules and put in place and connected on site. The primary and secondary modules are to be assembled but not permanently sealed at the assembly site. They will not be loaded with fuel or secondary salt during transport, and therefore pose no radiological hazard. Total module mass is reduced using this method, and fuel salt may be transported in a more secure manner, delivered to the site only when the system has been assembled and tested and is ready for fuelling. Power conversion equipment is very large and heavy and will require several transport operations for delivery. Components will be individually constructed and the power conversion system will be first assembled on site.

6.1.2 Module Transportation

One of the fundamental design premises was to be able to transport the reactor to a remote area or developing nation for assembly and operation. The transport constraint considered for transportation is 454 metric tons (500 US) on one heavy haul transport load. Specialized services provided by heavy rigging and transportation companies include cranes that can lift from 9 MT (10 US) to 544 MT (600 US) and the necessary equipment and expertise to handle movement of these components. An example is given in **Figure 18**.

Figure 18: Heavy Haul Over Land of 500+ US Ton Component

The task of moving 454 metric tons (500 US) is also possible by way of ship, if necessary, to get close to the destination of choice and then by either train or some type of heavy haul transporter. The one disadvantage of train is that in some emerging and remote areas, the necessary infrastructure may not be in place to support rail movement. The same may also be true of acceptable roads for heavy transportation but is more likely to exist than an existing rail to the selected location. In our design, either or both could be used to transport 454 MT (500 US) loads. An example of transportation is given in **Figure 19**.

Figure 19: Transportation Via Ship of 500 US ton Components

The mass of the primary containment system is determined first based on the containment structure, the vessel, primary piping and primary heat exchanger along with some allowance for parts of the system not described in detail in this project. The mass and volume of all primary module components are detailed in **Tables 12** through **14** along with totals.

Table 12: Data for Determining Fission Chamber Volume and Mass

Core Region	Material of Construction	Material Density (g/cc)	Radius I/O (m)	Height (m)	Volume (m^3)	Mass (kg)	Mass (MT)	Mass (US Ton)
Active Core	Graphite	1.74	0 / 1.5	4.8	30.53	59036.81	59.04	65.06
Reflector	Graphite	1.74	1.5 / 2.25	4.8	42.41	73796.01	73.80	81.33
Vessel Side Walls	Hastelloy - N	8.86	2.3 / 2.35	5.3	3.87	34299.08	34.30	37.80
Vessel Base	Hastelloy - N	8.86	0 / 2.35	0.05	0.867	7685.80	7.69	8.47
Inlet Plenum	Hastelloy - N	8.86	-	-	1.31	11606.60	11.61	12.79
Outlet Plenum	Hastelloy - N	8.86	-	-	1.06	9391.60	9.39	10.35
Total	-	-	-	-		195815.90	195.82	215.79

Table 13: Data for Determining Other Component Volume and Mass

Primary Component	Material of Construction	Material Density (g/cc)	Length / Width (m)	Height (m)	Wall Thickness (cm)	Region Volume (m^3)	Region Mass (kg)	Region Mass (MT)	Region Mass (US Ton)
Heat Exchanger	Carbon Composite	2.0	1.5 / 2.5	2.0	N/A	10	10000	10	11
HX Housing	Hastelloy - N	8.86	1.05 / 3.8	2.5	2	5	5711	5.7	6.3
Primary Containment	Carbon Steel	7.86	4.88 / 4.88	25	4	366.5	168401	168.4	186
Core Dump Tank	Hastelloy - N	8.86	4.7 / 4.7	2	3	44	23047	23.0	25
Total	-	-	-	-	-	-	207159	207.1	228.3

Table 14: Data for Determining Primary Piping Volume and Mass

Primary Component	Material of Construction	Material Density (g/cc)	Length (m)	Inside Radius (cm)	Outside Radius (cm)	Region Volume (m^3)	Region Mass (kg)	Region Mass (MT)	Region Mass (US Ton)
Hot Leg Piping	Hastelloy - N	8.86	11.5	25	27	0.39	3457	3.5	3.8
Cold Leg Piping	Hastelloy - N	8.86	11.5	25	27	0.39	3457	3.5	3.8
Dump Tank Piping	Hastelloy - N	8.86	2	50	53.175	0.2	1776	1.8	2.0
Total	-	-	-	-			8690	8.8	9.6

The secondary system, which is also housed in a module type containment and ready for assembly does not have the added weight of the vessel and head and less inventory in fuel salt. The major components included in the secondary module are the secondary piping, three smaller secondary heat exchangers and the secondary salt pump.

Also to be transported is the power conversion system that includes the helium piping and a series of three turbine generators, plus the additional recuperators, compressors and cooling equipment.

The transportation of the primary containment without the fuel salt would be able to be accomplished in one heavy haul transport load with a maximum of 454 MT (500 US). An additional load would be required for the secondary system and then an additional load(s) for the power conversion system.

6.1.3 Site Preparation and System Assembly

Site selection for the SMMSR is contingent upon several key naturally occurring features being readily available. One site specific limitation is that the primary containment module as proposed is to be placed into a silo to be trenched into the earth. This silo needs to be approximately 28 meters in depth and be approximately 25 square meters in area. The water table in most locations will likely occur above this level, and the SMMSR containment module shall be constructed to withstand moisture impingement on the outer surface. Other corrosive elements in the water need to be checked for. The stability of the supporting earth at that below grade level needs to be sufficient to support a concentrated 750+ US ton system. Seismic considerations need to be calculated, and a heat sink methodology needs to be considered. One of the many GNEP goals for the mobile deployable reactor program is that the system may support district heating or desalination projects. The system's heat sink can be incorporated into such processes. The site needs to be accessible via heavy haul transporter as discussed in section **6.1.2**.

First, silo preparation work needs to be performed including the delivery of heavy lifting and excavation equipment. The primary module will then be placed into the silo and then the secondary loop and power cycle equipment can then be assembled.

6.1.4 Start Up Preparations

The helium system is to be used for heat up and leak checking purposes. First the power cycle equipment is made fully functional. Then sufficient quantities of frozen FliBe are brought to the site. The salt is melted either via electrical heaters, helium heating, or by heating by combustion engine exhaust gas (diesel generator, or transport trucks) and used to fill the primary and secondary loops. The secondary circulating pump can be used to maintain the temperature of the two systems with pumping action. Leak checks and other preparations may be carried out as the system up to this point has no fissile inventory. Once all system preparations are complete, the 30 year inventory of UF_4 feedstock is placed into the fuel fluorination system. In accordance with the GNEP goal of assuring non-proliferation, the primary

containment module will be sealed and the shadow biological shield put in place to permanently seal the system off from human intrusion.

6.2 Full Power Operations

6.2.1 Start Up

The fluorination system then begins slowly adding uranium hexafluoride to the FliBe in the primary loop. As the fuel salt flows through the fission chamber, it will become critical and deposit heat into the system continuing to heat all components up until the proper mole fraction of UF_4 is added to raise the system to the regulating temperature of 1000K at the hot leg. Under these conditions, the SMMSR is in hot standby and ready for power operations.

6.2.2 Fuel Cycle and On Line Refueling

The fuel-cycle chosen for this reactor is based on uranium enriched below the weapons-grade limit (20%). The use of uranium in a thermal-spectrum reactor means that a conversion ratio of unity cannot be achieved, and periodic additions of fuel will be necessary for reactor operation. One of the profound advantages of the fluid fluoride fuel form is that fuel additions are exceptionally easy to make. Indeed, fuel can be added to the reactor on an essentially continuous basis, which makes it possible to hold excess reactivity to very low levels.

The basis for fuel addition is the valence structure of uranium. Uranium has two major valence states, +4 and +6. In uranium oxide, these two valence states correspond to uranium dioxide (UO_2) and uranium trioxide (UO_3). In uranium fluoride, these valence states correspond to uranium tetrafluoride (UF_4) and uranium hexafluoride (UF_6). Uranium found in nature is typically a mix of the two valence states. U_3O_8 is actually a combination of one UO_2 molecule and two UO_3 molecules.

Uranium tetrafluoride and uranium hexafluoride exhibit markedly different behaviors and these behaviors not only form the basis for their use in the reactor, but also for familiar processes such as uranium enrichment. UF_4 is stable in fluoride salt mixtures at very high temperatures. UF_6 is gaseous and volatile, and will come out of a fluoride salt solution beyond a certain concentration.

The initial fuel for the reactor will come directly from the enrichment plant as frozen UF_6. UF_6 has a low sublimation temperature and will be added to the lithium-fluoride/beryllium-fluoride fuel solvent through reduction. This will take place in a column where the bare solvent salt ($LiF\text{-}BeF_2$) and UF_6 are introduced at the bottom of the column, flowing upward. Hydrogen gas is also introduced in the column and reacts with the UF_6, combining with some of its fluoride ions to form HF gas. This reaction will reduce the UF_6 into UF_4, and "bond" the UF_4 into the solvent in its non-volatile state.

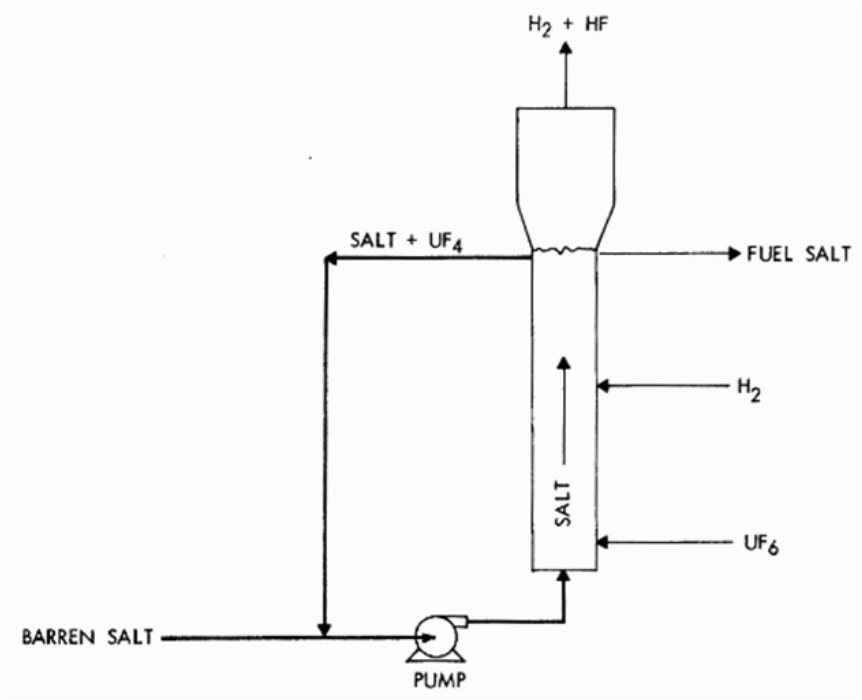

Figure 20: Salt Fluorination System

After the salt has reached its desired uranium fraction, the reactor can be taken to a critical configuration with essentially no excess reactivity. This configuration will not remain critical for very long, because the small amount of excess reactivity that is permitting criticality will soon be expended, and fission products will begin to accumulate in the fuel salt. These fission products will exert a poisoning effect that will further tend to drive down reactivity.

Normally, in a solid-core reactor, the reactor designers would have had to plan for all of these reactivity shifts and plan for sufficient excess reactivity to allow an acceptable fuel lifetime, typically several years depending on the fuel shuffling strategies. The large amount of excess reactivity would be carefully controlled through both control rod removal and chemical shim (boron) in the water.

The choice of a fluoride fuel form permits a much more elegant approach to these problems, and one that allows the reactor to "burn" the fuel essentially indefinitely. As reactivity drops due to fuel depletion and fission product buildup, additional reactivity in the form of new fuel is simply added to the fuel stream by the hydrogen reduction process previously described. Such a gentle application of fresh reactivity allows control rods and chemical shim to be eliminated from the reactor, along with all the attendant safety concerns that would follow a reactor design that depends on rods to control reactivity.

The use of UF_6 also allows the elimination of all fuel fabrication steps between enrichment and fuel utilization. Fuel can come directly from the enrichment plant in exactly the chemical configuration in which it was enriched, with no alteration. Such simplicity in design and operation is very important for a reactor that will be deployed to regions with little or no nuclear infrastructure.

The rate at which fresh fuel can be added to the primary salt can be controlled to an exceptionally fine degree using this technique, since the fuel is added in a gaseous form. The rate at which fuel is added to the reactor will be controlled by the same reactor control system that monitors reactivity and the reactor's balance temperature. The very long time scale at which fuel is added to the reactor, relative to its operating period, makes reactivity excursion events due to inadvertent fuel addition very unlikely.

And in the unlikely event the fuel addition system somehow got "stuck" open, and in the unlikely event that no operator did anything to prevent reactivity addition, the reactor's balance temperature would continue to increase until it exceeded the heat removal capability of the freeze valve at the bottom of the core vessel. The freeze valve would then thaw and the core salt would drain out of the vessel into the drain tank, shutting down reactor operation without damage or incident.

At the end of the reactor operation, fuel salt containing uranium, transuranics, and fission products will be drained from the reactor into the drain tank and allowed to cool for a reasonable period of time. Then this salt mixture, in accordance with GNEP principles, will be shipped back to the host country for reprocessing.

The reprocessing of the salt will be straightforward. First it will be fluorinated. This will remove all the uranium, neptunium, plutonium, and higher actinides as gaseous hexafluorides. Each of these can then be separately partitioned. Some of the fission products, such as molybdenum and technetium, will also come out of solution as gaseous hexafluorides. The remaining mixture of $LiF\text{-}BeF_2$ and fission product fluorides can then be decontaminated by distillation.

In the distillation process, the salt is heated to very high temperatures at reduced pressure. At these temperatures, the lithium fluoride and beryllium fluoride will become gaseous and come out of solution. They can then be condensed in a purified form and used in another fluoride reactor. The remaining mixture of fission product fluorides will be free of most of the solvent and all of the actinides, and can be disposed of in an appropriate manner.

6.2.3 Fission Product Control and Fluids Maintenance

6.2.3.1 Primary Salt

There will be an abundance of different fission products generated in the primary salt during the operation of the reactor, in a manner very similar to other thermal-spectrum reactors. These fission products can be broken down into three general classes.

First there are the fission products that are gaseous or have volatile fluorides. These include xenon, krypton, bromine, and iodine. Iodine forms a heptafluoride (IF_7) that is gaseous at reactor operating temperatures. These gaseous fission products will come out of solution as the salt makes its loop through the primary heat exchanger, and will be collected and cooled in an off-gas treatment system.

The short-lived isotopes of krypton and xenon will decay quickly into rubidium and cesium, both of which form very stable fluorides. Iodine will decay to xenon, freeing the seven fluoride ions that were bound to it in the transition. These fluoride ions will combine with the reactive rubidium and cesium formed from krypton and xenon decay, providing anions to these cations that had previously been noble.

In a similar manner, the second class of fission products in the salt are those that have stable fluorides that easily dissolve in the $LiF\text{-}BeF_2$ matrix. These fission products include the alkali metals and the alkaline earth metals such as rubidium, strontium, yttrium, zirconium, cesium, barium, and the lanthanides. These fission products will form very stable monofluoride, difluorides, and trifluorides that are non-volatile. The extreme chemical stability of these fluorides is especially important for fission products that pose special biological concern such as strontium (a bone-seeker) and cesium.

Finally the third class of fission products is the so-called noble metals, which do not form stable fluorides or form fluorides of weak stability. These include molybdenum, niobium, ruthenium, and tellurium.

These fission products will form volatile hexafluorides under exposure to additional fluorine, in a manner very similar to uranium, and could potentially be removed from the fuel salt by a simple fluorination scheme.

6.2.3.2 Secondary Salt

The secondary (coolant) salt is simply lithium-7 fluoride and beryllium-fluoride in a eutectic mixture. This salt has superior neutronic and heat transfer properties. Although the secondary salt is not exposed to the direct neutron flux of the core, it does intercept some delayed neutrons in the primary heat exchanger and needs to be compatible with the primary salt in the event of a leak into the primary system. No regular maintenance on the coolant salt is anticipated due to the lack of fission or activation products in the salt. An in leak of helium will not change salt composition. Tritium formed in the core from lithium will tend to diffuse into the secondary salt and from there into the helium of the power conversion system, where it will be removed.

6.2.3.3 Power Cycle Helium

The helium in the power conversion system is chemically and neutronically inert. Over time, tritium formed in the reactor from neutron-lithium interactions will diffuse into the helium of the power conversion system. In the helium loop it can be readily removed by a small introduction of oxygen into the helium. The oxygen will combine with the tritium to form tritiated water, which will condense in the precooler and can be removed in a straightforward manner.

6.3 Decommissioning

It is anticipated that at the end of the 30 year operational design life and coinciding with license termination, the SMMSR would be disassembled and the site returned to a state of unrestricted use as determined by 10CFR20, Subpart E-Radiological Criteria for License Termination.

6.3.1 Disassembly

The disassembly would take place very much like the original assembly, but in reverse order. The radioactive fuel salt would be drained into the drain tank in the bottom of the primary containment and allowed to cool until frozen for transportation. The power conversion system and secondary system would be uncoupled from the primary containment and dismantled back to the original shipping configuration.

The upper shadow biological shield would be removed from covering the primary containment. The primary containment would be capped at the penetrations where the secondary system was uncoupled and removed from the below grade silo with heavy lift cranes. The Core dump tank could be allowed to be separated from the primary containment module in order to simplify transport of the two assemblies. Barring any significant contamination issues, the primary containment module less the dump tank and fuel salt could be treated as class A waste, or possibly class B, but will not likely be considered greater than class C. On the other hand, the dump tank and fuel salt will be considered greater than class C and will require appropriate transport measures be taken. The frozen form of the fuel salt should somewhat simplify radiological containment concerns, though. Certainly, NRC regulations will need to be modified in order to reflect transport of spent fuel in this form.

6.3.2 Shipping

Without a radiological incident occurring over the operating life (no primary to secondary leaks as designed), the power conversion system and secondary system can be shipped as cargo without special restrictions using similar heavy transport equipment as was used for the original shipment.

The primary containment would need exclusive use transportation vehicles along with special arrangements and notifications made depending on the countries and states traversed. If necessary, there is also sufficient room for additional shielding for transportation and shipment before reaching the designed transportation limit of 500 tons. Shielding could be installed on the lower part of the primary containment to reduce workers' and transportation employees' exposure to As Low As Reasonably Achievable (ALARA) levels.

6.3.3 Site Release

The site would be returned to "as before" condition as much as possible. After removal of primary containment and all associated plant equipment, the site would be surveyed for release. The release limits in 10CFR20, Subpart E are quoted as:

§ 20.1402 Radiological criteria for unrestricted use.

A site will be considered acceptable for unrestricted use if the residual radioactivity that is distinguishable from background radiation results in a Total Effective Dose Equivalent (TEDE) to an average member of the critical group that does not exceed 25 millirem (0.25 milliSieverts) per year, including that from groundwater sources of drinking water, and the residual radioactivity has been reduced to levels that are as low as reasonably achievable (ALARA). Determination of the levels which are ALARA must take into account consideration of any detriments, such as deaths from transportation accidents, expected to potentially result from decontamination and waste disposal."

The hole excavated for primary containment would be refilled and the entire site landscaped to return it close to the original topography.

7.0 Design Rationale

The overall rationale of the reactor design is based on the overarching goal of a simple, reliable reactor than can provide 100 megawatts of electrical power in a system that can be transported by conventional means.

To achieve this goal, it was recognized from an early stage that the use of large pressure vessels in the primary core would be prohibitive from a weight and safety standpoint. This meant that only reactor designs that could utilize cores operating at ambient pressures could be reasonably considered. This effectively eliminated water-cooled or gas-cooled reactors from consideration, leaving reactors that utilized halide-salts or liquid-metals as a coolant as the only viable options for a reactor that had to achieve reasonable power conversion efficiency.

Another overarching consideration was the need to maintain reactivity in the reactor core over a period of decades without the replacement of fuel rods. This meant that a reactor had to breed new fuel at a rate commensurate with its consumption, or it had to have some particularly simple mechanism for reactivity addition. Naval nuclear vessels utilize highly-enriched uranium, but such an option was not available for this project due to nuclear material proliferation restrictions.

The two reactor options that our team came to very early in the design process were a solid-core, liquid-metal-cooled fast spectrum reactor and a fluoride-fueled, fluoride-cooled thermal spectrum reactor. The fluoride reactor could maintain its reactivity through the simple periodic addition of uranium in the form of uranium hexafluoride.

There were several basic advantages of the fluoride reactor over the liquid-metal cooled fast reactor that led us to choose this design. The ability to utilize a thermal neutron spectrum rather than a fast neutron

spectrum had important safety features in the form of stronger negative temperature coefficients of reactivity and longer reactor periods. Normally, the xenon transients that inhibit a thermal-spectrum reactor would have been of great concern, but the fluoride reactor allowed xenon to be removed online and the xenon effects were essentially eliminated.

There were important safety advantages to the fluoride reactor over the liquid-metal reactor. The fuel and coolant is chemically stable and will not react with air or water in case of accident, unlike the highly explosive and flammable liquid metal coolants. In the event of a loss-of-coolant accident the fluoride fuel would naturally drain into a passively cooled configuration, unlike the high-power density solid-fuel which must always be cooled by liquid-metal which could drain and react in case of accident.

Although not a primary concern, the chemical nature of the fluoride fuel meant that it could be used indefinitely, since it was not subject to radiation damage. This meant that any residual uranium remaining at the end of reactor operation, along with the fuel solvent, could simply be recycled easily to the next generation of reactors.

Table 15 summarizes key design parameters of the SMMSR. These and many other beneficial features of using a liquid fuel approach led our team to the conclusion that the advantages of the SMMSR make it a highly plausible approach for achieving the goals outlaid by the GNEP remote deployment reactor concept.

Table 15: Key Design Parameters of the SMMSR

System Parameter	Value	Units
Rated Thermal Power	240	MegaWatts
Rated Electric Power	100	MegaWatts
Calculated Thermal Efficiency	42.7	%
Primary Module Shipping Mass	410	Metric Tons
Primary Module Footprint	23.8	Square Meters
Primary Module Height	25	Meters
Primary Module Shipping Volume	595	Cubic Meters
Design Life Cycle	30	Years
Primary Coolant Outlet Temperature	1000	K
Neutron Spectrum	Epi-Thermal	-

8.0 List of References

1. D.F. Williams, L.M. Toth, K.T. Clarno, and C. W. Forsberg, "Assessment of Properties of Candidate Liquid Salt Coolants for the Advanced High Temperature Reactor (AHTR)" , Oak Ridge National Laboratory, Oak Ridge, TN, USA, June 30, 2005.
2. J.R. Engel, et al., "Conceptual Design Characteristics of a Denatured Molten Salt Reactor with Once Through Fuelling", ORNL/TM-7207, Oak Ridge National Laboratory, Oak Ridge, TN, USA, July, 1980.
3. P.F. Peterson, C. W. Forsberg, and P. Pickard, "Advanced CSiC Composites for High-Temperature Nuclear Heat Transport with Helium, Molten Salts, and Sulphur-Iodine Thermo chemical Hydrogen Process Fluids", Second Information Exchange Meeting on Nuclear Production of Hydrogen, Argonne National Laboratory, Illinois, USA, October 2-3, 2003.
4. P.F. Peterson, "Development of Liquid silicon Impregnated C/C SiC Composites for High-Temperature Heat Transport," U.C. Berkeley Department of Nuclear Engineering Report, UCBTH-03-100, October 2-3, 2003.
5. S. Subramanian, V. Ponyavin, C. De Losier, Y Chen, "Development of an Advanced High Temperature Heat Exchanger Design", Kick off Meeting for the Materials Consortium and The Design and Experimental Ventures, University of Nevada, Las Vegas, November 17, 2004.
6. R. F. D. Perret, "High Temperature Heat Exchanger Project", Quarterly Progress report, January 1 through March 31, 2004.
7. ORNL/TM-5325, 1976-04, "Evaluation of an Alternate Secondary (And Tertiary) Coolants for the Molten Salt Breeder Reactor.
8. C. W. Forsberg, P.F. Peterson, and H. Zhao, "An Advanced Molten Salt Reactor Using High-Temperature Reactor Technology" , 2004 International Congress on Advances in Nuclear Power Plants, June 13-17, 2004.
9. K. Nikitin, Y. Kato, L. Ngo, "Thermal-Hydraulic Performance of Printed Circuit Heat Exchanger in Supercritical CO CO_2 Cycle", Research Laboratory for Nuclear Reactors, Tokyo Institute of Technology, January 5, 2005.
10. Milan Nejedlý, Oldřich Matal, "Studies on Components for a Molten Salt Reactor", Transactions of the 17th International Conference on Structural Mechanics in Reactor Technology (SMiRT 17) Prague, Czech Republic, August 17 –22.
11. Code of Federal Regulations, Title 10, Part 20, Standards for Protection Against Radiation
12. Hastelloy®N alloy Technical Data sheet from Haynes International, Inc.
13. S.J. Zinkle, Summary of Physical Properties for Lithium, Pb-17Li, and (LiF)n•BeF2 Coolants, ORNL, APEX Study Meeting, Sandia National Lab, July 27-28, 1998

Appendix A: Reactor Design Methodology

The design of a nuclear reactor system can be complex and daunting. There are many inputs, constraints, limitations, and other concerns. It can be difficult to know which parameters to fix earlier in a design and which to vary to achieve an optimal system performance. Identifying those parameters which have a strong influence on the overall system is very important early in the design process, since it can reduce the number of iterations and analyses necessary to arrive at an attractive design.

A design tool called a design structure matrix (DSM) was utilized in this effort to help us visualize and understand the design space in which we worked. A design structure matrix is little more than a formalism that can be employed to allow a system engineer to visualize and rearrange a design process. Often it begins with little more than a list of design decisions written on a piece of paper. The designer then proceeds to link the design decisions to one another and observes the patterns that result. It often becomes clear to the designer, even at this very early stage, that a re-sequencing of design decisions can remove iterations. Another frequent realization is that additional constraints exist on a design that had not previously been identified. The very formalism of building a DSM is an excellent start to a design process, and it also helps other quickly and clearly follow the design logic.

The task of sizing the reactor vessel was necessary to begin neutronic analyses of the reactor. Therefore, it was necessary to identify the design inputs and constraints that would allow a preliminary reactor sizing calculation to take place. The formalism of a DSM proved to be very helpful in this task. The DSM used to arrive at this calculation is shown in **Figure 21** below.

This DSM shows the inputs and relationships between the different design inputs. The matrix is read from the upper left hand corner down to the lower right hand corner. The lines between the different boxes indicate relationships. Red boxes indicate primary inputs; green boxes indicate calculated or constrained data.

Beginning with the upper left hand corner, element 1 shows that the fuel salt is chosen to be lithium/beryllium/uranium fluoride. This constrains the next value, element 2, the liquidus (melting) temperature of the salt, which is a function of the composition. The coolant fluid, element 3, is chosen to be a eutectic of lithium and beryllium fluoride, which in a similar manner fixes the liquidus temperature of the coolant fluid, element 4.

The core outlet temperature, element 5, is a primary input in this design. Its only real constraints are the liquidus temperature of the core salt on the lower end and the boiling temperature of the salt on the upper end. The temperature differences across the countercurrent primary and secondary heat exchangers are also selected.

The core inlet temperature (element 7) can be calculated from the core salt liquidus temperature (element 2) and some thermal margin (element 6) to prevent freezing.

We assume that the gas heater inlet temperature (element 10) is simply the core salt inlet temperature (element 7) minus the temperature drops across the primary and secondary heat exchangers (elements 8 and 9). In a like manner, the gas heater exit temperature (element 11) is the core salt outlet temperature (element 5) minus the temperature drops across the heat exchangers.

1. Core Salt	7LiF-BeF2-UF4
2. Core Salt Liquidus	772. K
3. Coolant Fluid	LiF-BeF2 (66-34)
4. Coolant Fluid Liquidus	732. K
5. Core Outlet Temperature	1000. K
6. Thermal Margin	27. K
7. Core Inlet Temperature	799. K
8. Salt/Salt HX DT	20. K
9. Salt/Helium HX DT	20. K
10. Gas Heater Inlet Temperature	759. K
11. Gas Heater Outlet Temperature	960. K
12. Power Conversion System	helium gas turbine
13. Conversion Efficiency	42.2%
14. Helium Net Work	1.35 MW/kg/s
15. Electrical Power	100. MWe
16. Core Thermal Power	237. MWt
17. Helium Mass Flow Rate	76. kg/s
18. Coolant Fluid Mass Flow Rate	507. kg/s
19. Core Salt Mass Flow Rate	423. kg/s
20. Graphite Temperature	1050. K
21. Graphite Design Fluence	2.68^22 n/cm2
22. Core Lifetime	30.0 yr
23. Core Power Density	5.2 kW/L
24. Core Volume	45529. L
25. Core Diameter	300. cm
26. Core Length	644. cm
27. Core Height/Diameter	214.7%

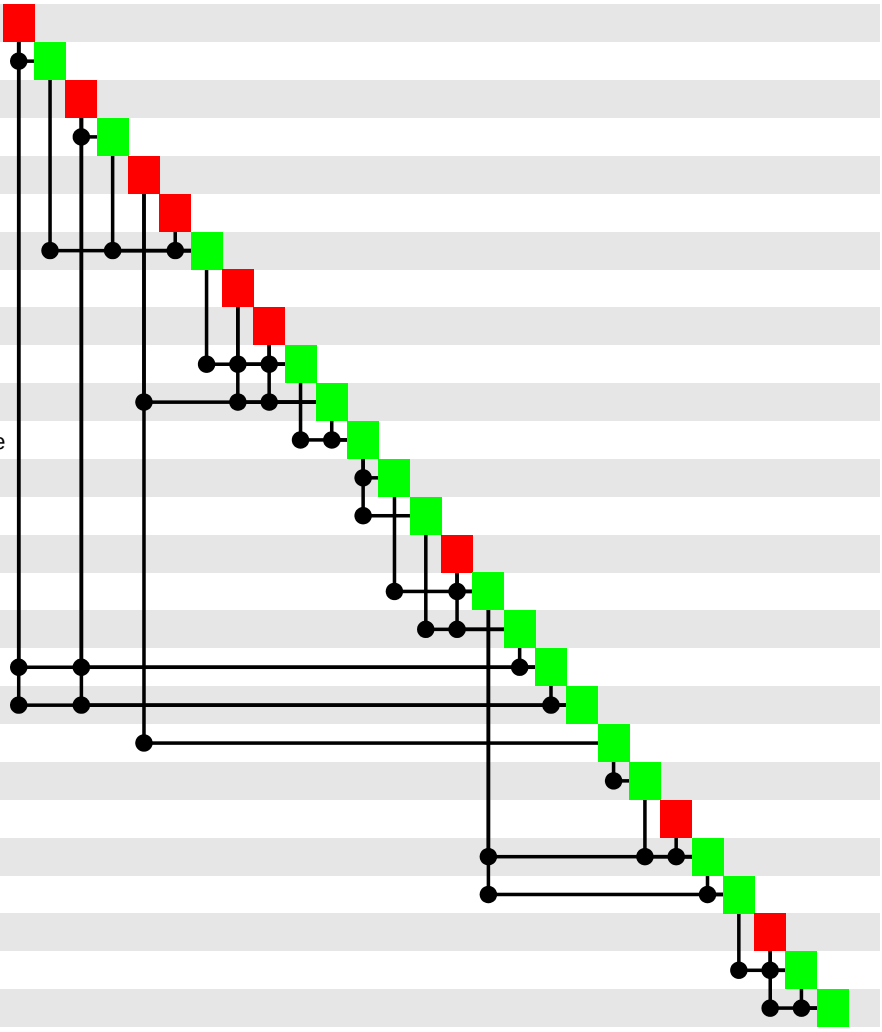

Figure 21: Visualization of a Design Structure Matrix

The power conversion system (element 12) is specified as a closed-cycle gas turbine using helium as the working fluid. In Appendix B an entire design technique for the helium gas turbine will be described, but the power conversion system will simply be treated as a "black-box" in this section. This calculation of the power conversion system performance yields conversion efficiency (element 13) and the net power per unit mass flow rate, or net work of the cycle (element 14).

Next the electrical power desired by the reactor is chosen (element 15). One might have thought that this would be a more primary input, perhaps taking a higher position in the design structure matrix, but one of the things that can be deduced from this formalism is that the choice of overall electrical power generation has not been required heretofore in the design process. That is, the calculations that have been made up to this point would be just as relevant for a 1000 MWe reactor or a 10 MWe reactor as they will be for a 100 MWe reactor.

Using the desired electrical power and the conversion efficiency of the system, it is easy to calculate the required core thermal power (element 16) of the reactor. In a similar manner, from the desired electrical power and net work of the cycle, the mass flow rate of helium is calculated (element 17).

A knowledge of the specific heat capacity of the coolant fluid, as well as a knowledge of the overall change in temperature of both the helium and the coolant fluid across the gas heaters, allow a calculation

to be made of the mass flow rate of coolant fluid in the secondary loop (element 18). This mass flow rate is significantly higher than the helium mass flow rate for several reasons. The first is that helium has a greater heat capacity per unit mass than the salt selected as the coolant fluid. The other reason is that the same helium flow is heated three times in the power conversion system by the coolant fluid, so that even if the coolant fluid and the helium had the same heat capacity, it would require roughly three times the flow rate of coolant fluid to achieve three heating passes through the helium. The core salt mass flow rate (element 19) is calculated based on the mass flow rate of the coolant fluid and the ratio of the specific heats of the core salt and coolant fluid.

Next the graphite temperature (element 20) is calculated from the core outlet temperature. This calculation is rather rough and is based on data taken from documents at ORNL describing the difference between the maximum temperature of the core salt and the maximum temperature of the graphite moderator. It is dependent on the geometry of the graphite prisms, their locations in the reactor, and the neutron and gamma flux in the graphite. This complex calculation is beyond the scope of this effort at the current time, and so based on analogy to published data, the maximum graphite temperature was taken to be 50 °C greater than the core outlet temperature.

From the graphite temperature, a relationship can be used, again based on ORNL experimental data, as to the maximum neutron fluence (element 21) that the graphite can experience before it begins to swell beyond its original dimensions. These relationships for graphite are described in detail in Appendix C. They are strongly dependent on temperature and on the allowable dimensional change, which for this design was given as zero. Based on these expectations, graphite at 1050K can withstand a fluence of 2.7 x 10^{22} neutron/cm^2 over its operational lifetime.

Next a core lifetime (element 22) is selected. Again, this was a primary input to the design, and given in the design problem as thirty years. In a worst-case scenario, graphite at 1050K, with the fluence limit previously given, can support a power density (element 23) of only 5.2 watts per cubic centimeter, or 5.2 kilowatts per liter, and maintain its dimensions over the given lifetime. This power density is significantly lower than a pressurized-water reactor or a sodium fast reactor, but those reactors don't have fuel that must operate for thirty years.

We recognize that this power density calculation leads to an artificially low power density. The maximum flux will not be experienced in the same region of the core where the maximum graphite temperature is achieved. Nevertheless, it is a valuable calculation for rough sizing of the reactor, assuming a reactor that has achieved perfect radial and axial flux flattening.

From the core power density and core power values, a calculation of core volume (element 24) is straightforward. When combined with a constraint on core diameter (element 25), which was chosen for this design to be three meters, a calculation of core length (element 26) can be made, in this case roughly six meters.

Appendix B: Power Conversion System Calculations

A gas turbine power conversion system utilizes the compression of a gas at low temperatures followed by the addition of heat and expansion at high temperatures to produce net work. A closed-cycle gas turbine also involves the removal of heat and the recompression of the original working fluid at lower temperatures. Further improvements to the closed cycle involve the use of regeneration, intercooling, and gas reheated in between stages of expansion.

This project required modification to the standard techniques of closed-cycle gas turbine power cycle design to accommodate particular constraints levied by the heating fluids, namely their melting temperatures. This restricted the minimum temperature at which heat could be added to the working fluid (gas). To minimize iterations, a new design strategy was implemented where gas heater inlet temperature became a primary input rather than overall cycle pressure ratio, a much more conventional design parameter.

To illustrate the design process, a design structure matrix (DSM) was created for the power conversion system. This DSM serves as a sub design to the overall reactor design structure matrix, receiving inputs from the overall DSM and generating outputs.

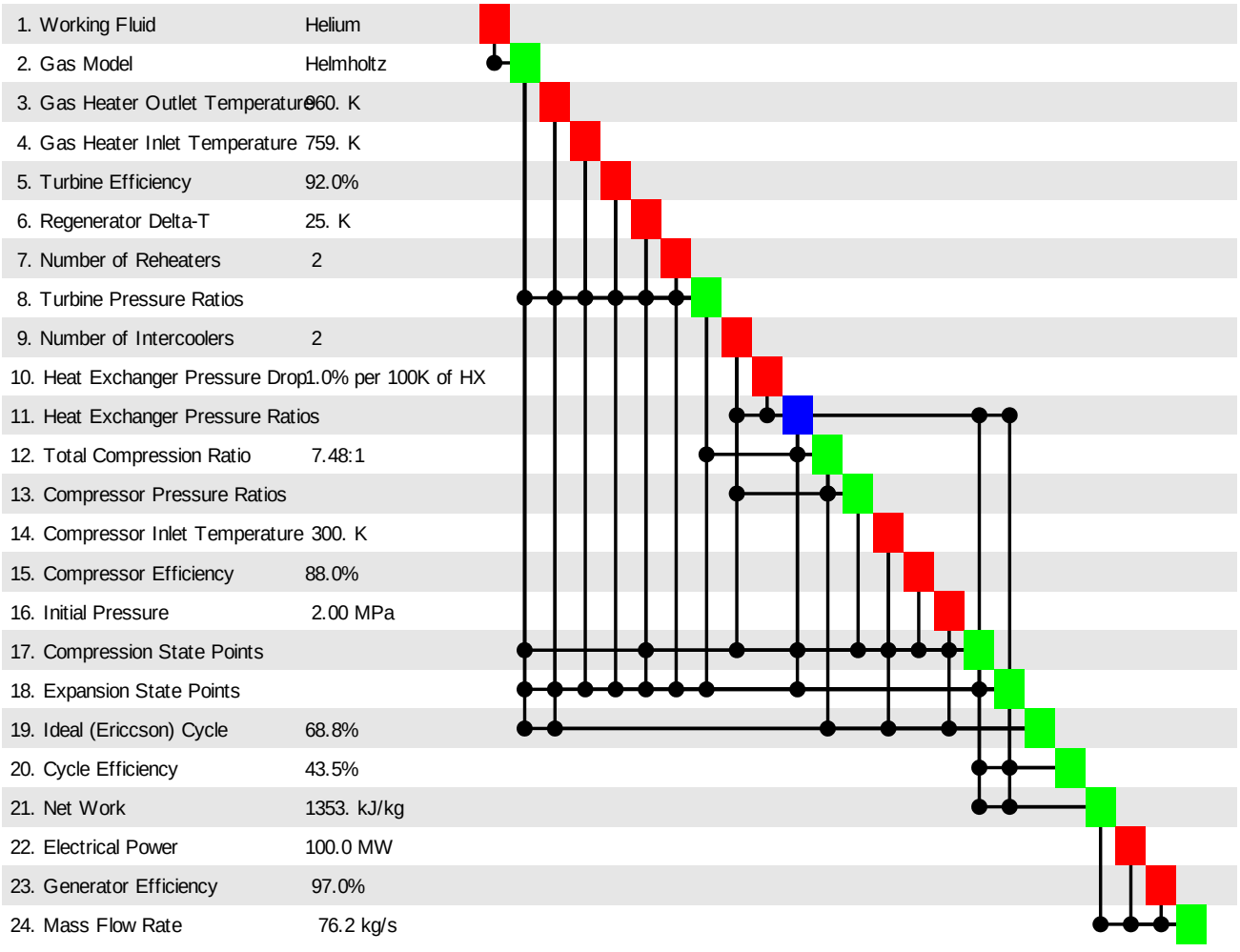

Figure 22: DSM for Gas Turbine PCS Constrained by Gas Heater Inlet and Outlet Temperatures

In a similar manner to the reactor system DSM, the modeling begins with the selection of the working fluid (element 1) and a gas model for this working fluid (element 2). In this case, a Java model of the gas, using the Helmholtz equations-of-state, was developed and utilized. The gas model allows the state of the gas to be calculated given different pairs of state point data (pressure and temperature, pressure and enthalpy, pressure and entropy, and so forth). Without the gas model, a designer would be forced to employ table lookups and interpolations for each state point desired. Such a technique does not lend itself well to the rapid and accurate iterations needed in such a complex model.

Next follow five design inputs. The gas heater outlet temperature (element 3), the gas heater inlet temperature (element 4), the turbine efficiency (element 5), the temperature difference across the regenerator (element 6), and the number of reheating stages (element 7) are all necessary to make the first set of calculations, the pressure ratios across the turbine stages.

Typically, a cycle that employs reheating stages finds that optimal performance is achieved by keeping the pressure ratios across each stage identical. This would be followed in this model except for one issue—this leads to different temperature rises across the heating stages. This is because of inevitable inefficiencies in the regenerator. The regenerator is the heat exchanger that transfers enthalpy from the low-pressure exhaust of the final turbine stage to the high-pressure flow leading to the first turbine. Since any heat exchanger inevitably involves heat transfer across some temperature difference, it follows that the incoming high-pressure gas flow will not be able to be heated up to the same temperature as the low-pressure exhaust. In such a case, the temperature rise across the first heating stage will be larger than the temperature rise across the other heating stages. In the heating fluid (which in our case is a fluoride salt) this will mean that one of the salt flows will emerge from the gas heater at a lower temperature than the other two streams, and mixing of the three streams will take place that will lead to heat loss from the two hotter streams.

An alternative to three different salt flows at different temperatures would be to alter the pressure ratios across the turbines so that the temperature rise across each heating stage is identical. Such a calculation can be made by utilizing isentropic relationships correlating pressure ratio and temperature ratio, and then accounting for turbine inefficiencies to calculate actual pressure ratio for a given temperature ratio.

To find the pressure ratio across a turbine, one must first know the initial and final temperatures of an isentropic expansion. But for this design, the actual gas heater inlet temperature (turbine exhaust temperature) and gas heater outlet temperature (turbine inlet temperature) are known. To find the isentropic turbine exhaust temperature, we make use of the definition of turbine efficiency in an adiabatic condition (a turbine expansion where no heat is transferred into or out of the turbine during the expansion process).

Equation 8: Adiabatic Turbine Efficiency

$$\eta_{turbine} = \frac{h_1 - h_{2a}}{h_1 - h_{2s}} \approx \frac{c_p\left(T_1 - T_{2a}\right)}{c_p\left(T_1 - T_{2s}\right)} = \frac{T_1 - T_{2a}}{T_1 - T_{2s}}$$

In **Equation 8**, $\eta_{turbine}$ is the adiabatic turbine efficiency, h_1 is the enthalpy at the turbine inlet, h_{2s} is the enthalpy at the turbine exit after an isentropic expansion, and h_{2a} is the actual enthalpy at the turbine exit after an actual expansion. If we further make the assumption of an ideal gas (an excellent assumption for helium at these temperatures), then the values of enthalpy can be replaced with values of temperatures, since enthalpy is only a function of temperature for an ideal gas.

With this assumption, and the temperatures at the turbine inlet and actual exit known (by virtue of knowing the gas heater inlet and outlet temperatures), as well as a knowledge of the adiabatic efficiency of the turbine, it is straightforward to calculate the isentropic turbine exit temperature.

Equation 9: Isentropic Turbine Exit Temperature

$$T_{2s} = T_1 + \left(\frac{T_{2a} - T_1}{\eta_{turbine}} \right)$$

Once the isentropic turbine exit temperature is known, the pressure ratio across the turbine can be calculated by the isentropic relationship between pressure ratio and temperature ratio.

Equation 10: Isentropic Pressure Ratio

$$\frac{p_1}{p_2} = \left(\frac{T_1}{T_{2s}} \right)^{\frac{\gamma}{\gamma - 1}}$$

In **Equation 10**, p_1 is the inlet pressure to the turbine, p_2 is the exit pressure from the turbine, and γ is the ratio of specific heats in the gas, which for a monatomic gas like helium is simply 5/3.

For each of the first two turbines, the turbine inlet temperature is simply the gas heater exit temperature, and the actual turbine exit temperature (T_{2a}) is simply the gas heater inlet temperature. But for the final turbine stage, the actual turbine exit temperature should be adjusted upward by the temperature difference across the regenerator in order to yield a pressure ratio that will keep the enthalpy addition across all gas heaters constant.

Equation 11: Actual Exit Temperature for the Final Turbine

$$\left(T_{2a}\right)_{finalturbine} = T_{gas-heater-inlet} + \Delta T_{regenerator}$$

With the pressure ratios across each of the turbine stages calculated, attention can then be turned to the compression system. The compression system must generate the pressures for each of the turbines, as well as any of the pressure losses across the heat exchangers in the system.

To simplify the problem, the pressure loss across each heat exchanger is assumed to be an exponential function of the enthalpy exchange of the surface, which is simply a temperature difference, based on the correlation between temperature and enthalpy in an ideal gas. For the first iteration, however, the temperatures at each of the state points in the cycle are unknown, and so even this approximation at pressure loss cannot be made.

In order to begin the calculation, an assumption of no pressure loss across heat exchanger surfaces is made. This enables a "first pass" through the state points of the cycle, and the state points can then be used for a pressure loss calculation and the calculation repeated.

For the first iteration, the pressure ratio across the compression system is simply the product of all the pressure ratios across the turbines. The assumption is made that each turbine stage is mounted on a shaft that drives both a generator and one or more stages of compression. Therefore, three turbines will drive

three generators and at least three compressors, each separated by a cooling stage. It is conceivable that each turbine stage might drive one or more stages of compression, separated by cooling stages.

Assuming that each of the compression stages has an identical pressure ratio, the individual pressure ratio of each compression stage is simply the nth root of the overall compression ratio, where n is the number of compression stages.

Next come three design inputs that govern cycle performance. First is the compressor inlet temperature (element 14). Compressor inlet temperature is the key to overall cycle performance, since it defines the minimum temperature in the cycle and is paramount to determining the efficiency of the cycle, as well as its performance relative to the bounds of the ideal Carnot cycle. Next compressor efficiency (element 15) is specified, followed by the compressor inlet pressure (element 16). Compressor efficiency is very important to cycle performance, but compressor inlet pressure has a nearly negligible effect on cycle performance. Compressor inlet pressure can be varied with little effect to efficiency or net work. What is especially appealing about compressor inlet pressure is that it basically serves as a "sizing" term that can be used to scale the turbomachinery up and down in size according the preference of the designer, with almost no effect on the cycle. The benefit of such a sizing parameter can scarcely be overestimated.

With the pressure ratios across each compressor known, as well as the compressor efficiency and compressor inlet temperatures, a calculation of compressor state points can be made using the gas model.

Such a calculation begins at the inlet to the first compressor, where both pressure and temperature are known. The gas model is queried to provide the other state variables at this point. Next an isentropic expansion to a higher pressure is modeled. The higher pressure is simply the inlet pressure multiplied by the pressure ratio across the first compressor. Entropy is assumed to be the same since this is an isentropic process. The gas model is queried again, this time with a new pressure and the same entropy as the two state points.

Since the gas expansion is not really isentropic, the inevitable compressor inefficiencies must be accounted for using a simple ratio.

Equation 12: Adiabatic Compressor Efficiency

$$\eta_{compressor} = \frac{h_{2s} - h_1}{h_{2a} - h_1}$$

Where $\eta_{compressor}$ is the adiabatic efficiency of the compressor, h_1 is the gas enthalpy at the compressor inlet, h_{2s} is the gas enthalpy after an isentropic expansion, and h_{2a} is the actual enthalpy after a non-isentropic expansion.

h_{2a}, the enthalpy after a non-isentropic expansion, is the quantity of interest in the calculation, since inlet enthalpy and isentropic outlet enthalpy have been calculated from previous queries to the gas model.

Equation 13: Actual Enthalpy at the Compressor Exit

$$h_{2a} = \frac{h_{2s} - h_1}{\eta_{compressor}} + h_1$$

With the actual enthalpy after a non-isentropic expansion so calculated, the gas model is again queried, this time with pressure and enthalpy as the state inputs.

If there are additional stages of compression, then the gas must be cooled across a cooling stage before further compression. If there is a pressure drop across the cooling stage, then the compressor outlet/cooler inlet pressure is multiplied by this pressure ratio (which will be less than unity) to calculate the pressure at the cooler outlet/next compressor inlet. The temperature at the cooler outlet is assumed to be the same as the overall compressor inlet temperature, representing the temperature removal capability of the heat sink and the lowest temperature of the cycle. With the cooler outlet pressure and compressor inlet temperature as the state points, the gas model is again queried to provide state point values.

The previous procedure is then repeated for each stage of compression, until the last stage is reached. The last stage does not lead to a cooling stage, but rather to the regenerator, where enthalpy is exchanged between the high-pressure gas flow and the low-pressure gas flow leaving the last stage of expansion. This point, however, marks the end of the calculations on compression state points.

Attention now turns to the calculation of the expansion state points. The starting state point is the inlet to the first turbine. The pressure at the first turbine inlet is found by taking the pressure at the last compressor exhaust and multiplying it by the pressure ratio across the high-pressure leg of the regenerator and the pressure ratio across the preheater (the first heating stage). The temperature is simply the turbine inlet temperature, or the gas heater exit temperature.

Now a very similar arrangement is followed to the compression system. An isentropic expansion is calculated, and the properties of the new state point are obtained from the gas model. Then a correction for turbine efficiency is applied, leading to a new state point defined by pressure and enthalpy. Finally, the gas is either reheated to the turbine inlet temperature (gas heater exit temperature) or it enters the low-pressure side of the regenerator. The pressure ratios previously calculated for each turbine stage are used calculate the state points of the expansion system.

The final remaining task is the calculation of state points for the high- and low-pressure regenerator exhausts. The regenerator inlet conditions are already known from the last compressor exit and the last turbine exit. The regenerator outlet conditions can be found very easily by assuming that the outlet conditions are at the same temperature as the inlet conditions less the temperature difference across the regenerator. Note that the temperature differential is between the low-pressure regenerator inlet and the high-pressure regenerator exit, and the low-pressure regenerator exit and the high-pressure regenerator inlet.

Equation 14: Regenerator Exit Temperatures

$$T_{hi-press-regen-exit} = T_{low-press-regen-inlet} - \Delta T_{regenerator}$$

$$T_{low-press-regen-exit} = T_{hi-press-regen-inlet} + \Delta T_{regenerator}$$

With all the state points for the compression and expansion systems calculated, it is a simple matter to tally enthalpy changes across coolers and heaters and do a cycle efficiency calculation (element 20). Net work (element 21) can also be calculated by tallying the turbine work and subtracting the compressor work. The DSM shows an iteration on the heat exchanger pressure ratios (element 11) based on the state points from the compression and expansion systems (elements 17 and 18). Iteration is indicated by the blue color of the box at element 11, showing that it is dependent on downstream data in order to make a calculation. Any time an iteration is present, an initial guess will have to be made in order to proceed

with the calculation. As was previously mentioned, the initial guess for heat exchanger pressure ratios was simply that each of them were unity, in other words, that there was no pressure loss across the heat exchanger. After a first calculation of state points, the heat exchanger pressure ratios can then be approximately calculated, and the overall cycle calculation rerun until an acceptable convergence is achieved.

Once convergence is achieved, then only a few calculations remain. Inputs for electrical power (element 22) and electrical generator efficiency (element 23) are given in order to make a calculation for the mass flow rate of helium through the system (element 24). As was shown previously, these values of efficiency and mass flow rate are then used in the reactor design sequence to compute other values of importance to the overall design.

Appendix C: Graphite Dose and Fluence Calculation Methodology

The performance of graphite in a high-temperature, fluoride salt reactor has profound implications for the design and operation of the reactor. Graphite has some unique properties in the fluoride reactor:

- It is stable at the high-temperatures at which the fluoride reactor operates, neither dissociating nor undergoing phase-change.
- It has an exceptionally small neutron absorption cross-section which enables high neutron economy.
- Fluoride salt does not attack graphite—it is chemically stable.

Despite the fact that graphite cannot moderate neutrons nearly as well as hydrogen or deuterium, these special properties enable unclad graphite to serve as an attractive moderator for a fluoride reactor.

However, prolonged exposure to fast neutrons causes changes in the crystalline structure of graphite. Initially, the graphite will contract as voids that were generated during fabrication close. The graphite will reach a minimum volume and then begin to expand as fast neutrons displace carbon nuclei from their graphite lattice positions. This contraction and expansion behavior is a strong function of both the temperature of the graphite (which governs lattice mobility) and the fast neutron fluence to which it is exposed.

Although most fluoride reactors utilizing graphite moderation favor a thermal neutron spectrum, the neutrons born from fission must be slowed down from their initial high-energies through collisions with carbon nuclei, and hence a fast flux is seen even in an otherwise thermal spectrum reactor. Such issues with graphite would present themselves in other reactors that used graphite moderation, such as a gas-cooled prismatic or pebble-bed reactor, but in these reactors the fuel typically is the lifetime limiter rather than the graphite. In the fluoride reactor, with its fuel form that is impervious to radiation damage and the ability to add or remove reactivity online, the graphite itself tends to become the lifetime limiter.

It was very important in our reactor design to understand and model the effects of graphite dimensional change on core lifetime and allowable fluence. A literature search was undertaken and a number of excellent papers from Oak Ridge National Laboratory on the subject were discovered. The paper of particular interest that yielded the data and correlations for this appendix was ORNL-TM-2136, "Graphite Behavior and its Effects of MSBR Performance", written in February 1969.

To understand the performance in graphite in a fast flux, the authors used irradiation data of graphite samples in the Dounreay Fast Reactor in Scotland in the mid-1960s. These data yielded a series of curves of graphite dimensional change as a function of neutron fluence and graphite temperature which are shown in **Figure 23**.

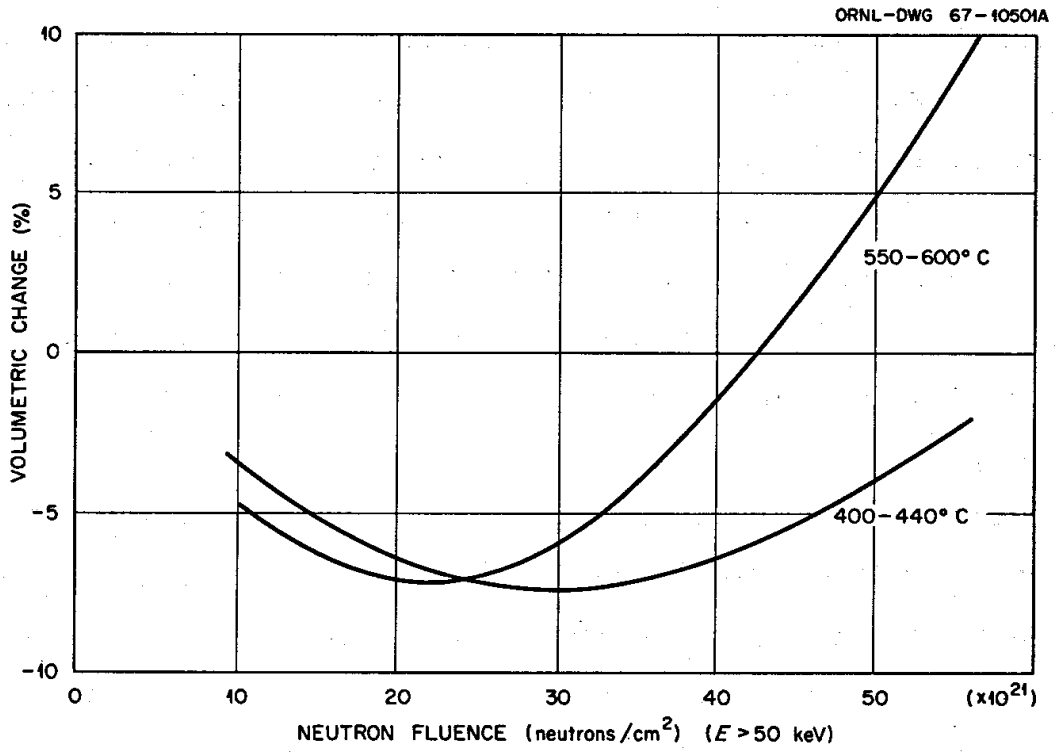

Figure 23: Graphite Dimensional change VS Fluence and Temperature

From page 18 of ORNL-TM-2136, the Dounreay data was condensed into an expression for the dimension length change of isotropic graphite as a function of neutron fluence and temperature:

Equation 15: Isotropic Graphite Dimension Change VS Fluence and Temperature

$$\frac{d\ell}{\ell} = \frac{1}{3}\left(0.11 - 0.00007\,T\right)\left(x^2 - 2x\right)$$

Where $d\ell/\ell$ is the non-dimensional change in length, T is the temperature in degrees Celsius, and x is found from the expression:

Equation 16: Definition of Variable "x" in Equation 8

$$x = \frac{\phi t\left(10^{22} n/cm2\right)}{5.7 - 0.006T}$$

Where φt is the fast neutron fluence and T is the temperature in degrees Celsius.

When plotted as a function of fluence with temperature as a parameter as shown, $d\ell/\ell$ is a strong function of the irradiation temperature.

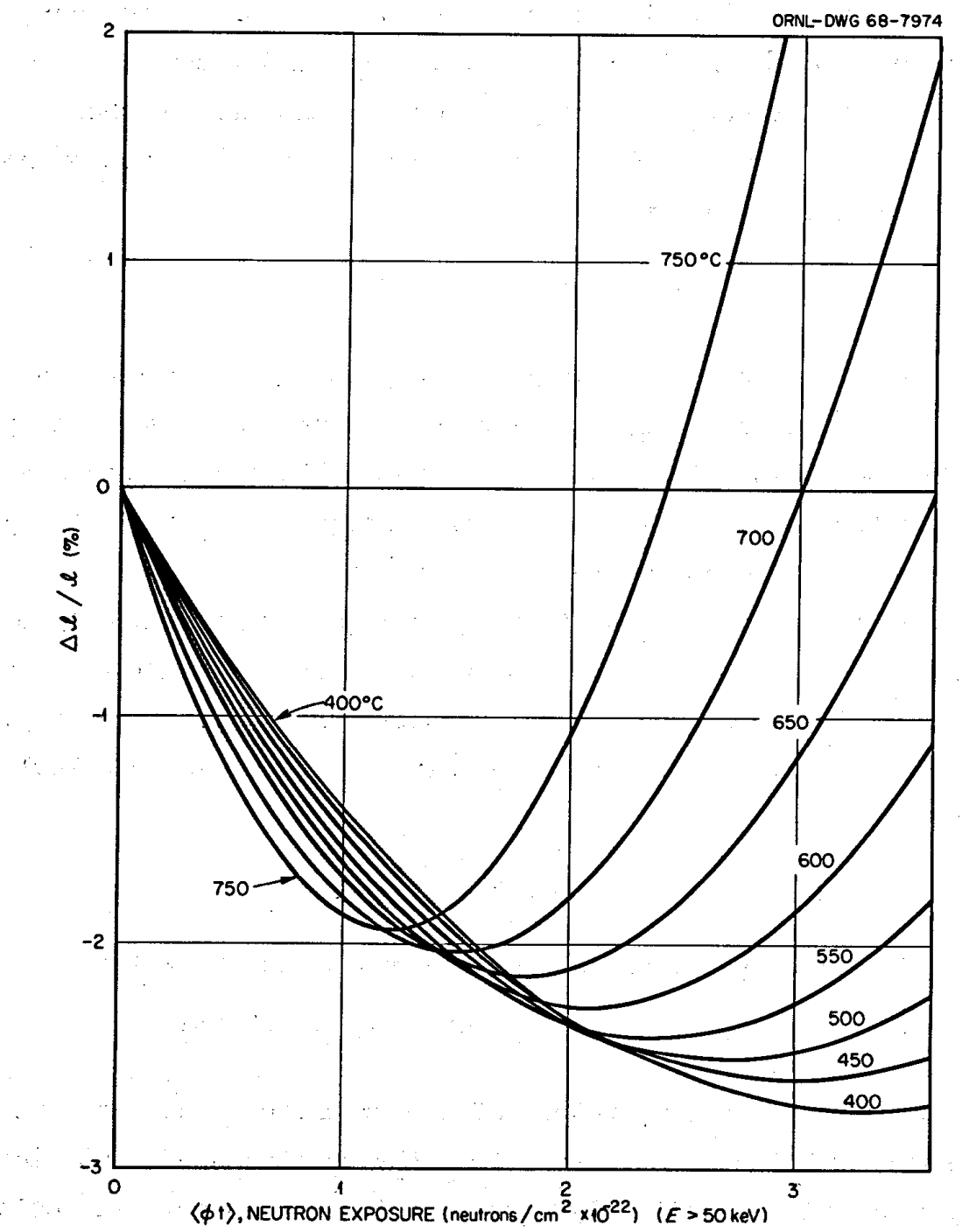

Figure 24: Isotropic Graphite Dimension Change (dℓ/ℓ) VS Fluence and Temperature

To solve this expression for fluence instead of for dimensional change, let us rename some of the portion of the expression:

Equation 17: Definition of a(T)

$$a(T) = \frac{1}{3}(0.11 - 0.00007\,T)$$

Equation 18: Definition of b(T)

$$b(T) = 5.7 - 0.006T$$

Then the original expression can be rewritten as:

Equation 19: Rewritten Version of Equation 8

$$ax^2 - 2ax - \frac{d\ell}{\ell} = 0$$

Which can be solved for the variable x by the quadratic formula, yielding:

Equation 20: Solution Function for x of Equation 12

$$x = 1 + \sqrt{1 + \frac{d\ell/\ell}{a(T)}} = \frac{\phi t\left(10^{22} n/cm2\right)}{b(T)}$$

The fast fluence is then:

Equation 21: Fast Fluence as a Function of a(T) (Equation 10) and b(T) (Equation 11)

$$\phi t\left(10^{22} n/cm2\right) = b(T)\left(1 + \sqrt{1 + \frac{d\ell/\ell}{a(T)}}\right)$$

To correlate fast fluence to core power density and lifetime, we use a data point from page 4 of ORNL-TM-2136:

> "On this basis, and considering results obtained to date with present-day graphites, the permissible exposure under MSBR conditions is estimated to be about 3.0 x 10^{22} nvt (E > 50 kev) at an effective temperature of 700°C. More specifically, at a peak core power density of 100 kW/liter under MSBR operating temperatures, return of the graphite to its original volume corresponds to about 2.5 years of reactor operation a 90% load factor."

Using this information, we can construct a correlation between fluence, lifetime, and core power density, assuming that fluence and lifetime are given and core power density is desired:

Equation 22: Correlation between Fluence, Lifetime, and Core Power Density

$$powerdensity = (100kW/L)\frac{\phi t}{\left(3.0x10^{22} n/cm2\right)}\frac{(2.25\, fullpoweryears)}{lifetime(FPY)}$$

Using the previous definition for fluence and removing the units:

Equation 23: Rewritten Version of Equation 15

$$powerdensity = (100kW/L)\left(\frac{2.25FPY}{lifetime(FPY)}\right)\left(\frac{b(T)\left(1 + \sqrt{1 + \frac{d\ell/\ell}{a(T)}}\right)}{3.0}\right)$$

Finally, by fully expanding the expression, we get:

Equation 24: Expansion of Equation 16

$$powerdensity = (100kW/L)\left(\frac{2.25FPY}{lifetime(FPY)}\right)\left(\frac{(5.7-0.006T)}{3.0}\left(1+\sqrt{1+\frac{3d\ell/\ell}{(0.11-0.00007T)}}\right)\right)$$

Equation 24 yields the power density, in kW/liter, that gives the desired moderator lifetime (in full-power-years) at the desired temperature (in degrees Celsius) for the desired dimensional change.

Figure 25 shows some results for core power density based on zero-net-distortion and variable graphite temperatures and lifetimes:

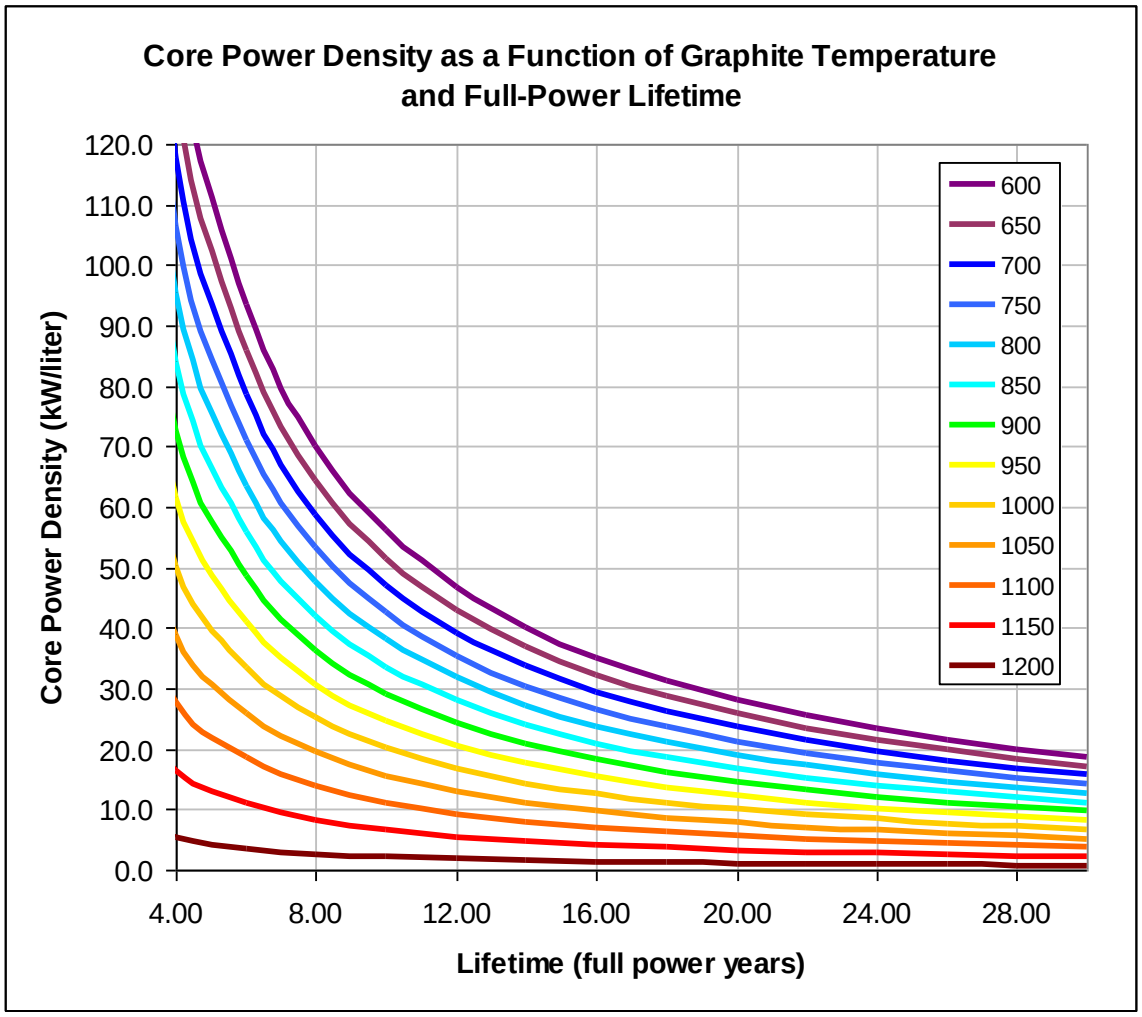

Figure 25: Core Power Density with Variable Graphite Temperatures and Lifetimes